E-20-E47

Extension of Direct Sensitivity Analysis to Particulate Matter Dynamics and Wet Deposition

James W. Boylan, Mehmet T. Odman, James G. Wilkinson and Armistead G. Russell
School of Civil and Environmental Engineering, Georgia Institute of Technology, 200 Bobby Dodd Way, Atlanta GA 30332-0512

Yueh-Jiun Yang
California Air Resources Board

Stephen F. Mueller and Robert E. Imhoff
Tennessee Valley Authority, PO Box 1010, Muscle Shoals, AL 35662

Abstract – A direct sensitivity analysis technique (DDM-3D) has been integrated into the URM-1ATM three-dimensional air quality model to efficiently provide an indication of which emission source types from various source areas have the greatest potential to impact pollutant levels. In this study, nine episodes were modeled to represent annual aerosol and wet deposition levels. Direct sensitivity analysis was then used to quantify the source/receptor relationship between emissions from thirteen geographic regions and pollutant levels in the Southern Appalachian Mountains (SAM). In particular, the impact of SO_2 emission reductions on aerosol and wet deposition levels at ten Class I areas are discussed. SO_2 emission reductions from different geographic regions displayed very different levels of impact on various sites within the SAM region. In general, the receptor sites showed the greatest response to emission reductions in the nearest states and regional sub-domains. Sites in Alabama and Georgia show the greatest response to reductions in emissions from Alabama and Georgia, respectively. The sites in North Carolina and Tennessee show the greatest response to emission reductions in Tennessee. And, the sites in Virginia and West Virginia show the greatest response to emission reductions in Virginia, West Virginia, and the Midwest sub-domain.

Keywords: air quality, sensitivity analysis, particulate matter, deposition, regional modeling

INTRODUCTION

Elevated levels of particulate matter, acid deposition, and ozone adversely impact visibility, streams, soil and vegetation (Sisler and Malm, 2000; Cowling, 1989; Heck *et al.*, 1998) in the Class I areas (national parks that are greater than 6,000 acres and wilderness areas greater than 5,000 acres) of the Southern Appalachians. However, the relative contribution of emissions from different geographical areas to the regional air pollution problem is not well quantified

Sensitivity analysis is a powerful tool for identifying and quantifying the impacts

of inputs (e.g. emissions) and system parameters (e.g. rate constants) on air quality modeling results. Sensitivity analyses are performed at all stages of the modeling process and can be used to determine the response of models to various configurations and inputs, explain model performance, improve reliability of predictions, or analyze the impacts of various control strategies (USEPA, 1999). Traditionally, a "brute-force" approach has been used to calculate sensitivities of pollutant concentrations to various parameters. This method involves running the model a number of different times, each time perturbing one parameter and comparing the results to the original run. On the other hand, embedding a direct sensitivity technique into the model allows the user to perform numerous sensitivity calculations in one model run. The Decoupled Direct Method (Dunker, 1981 and 1984) is one such technique that directly calculates sensitivity coefficients by taking the derivatives of the governing equations. The Decoupled Direct Method was successfully implemented into the CIT (California/Carnegie Institute of Technology) three-dimensional photochemical air quality model (Russell et al., 1988; Harley et al., 1993) by Yang et al. (1997) and was used to estimate sensitivities of ozone concentrations to initial conditions, dry deposition velocities, reaction rate constants, wind speeds, and emissions. The application of this technique is called the Decoupled Direct Method for three-dimensional models (DDM-3D).

Most of the sensitivity analysis in the past has focused on the effect of NO_x and VOC emission reductions on ambient ozone concentrations. Minimal work has been undertaken to address how fine aerosol particles and wet acid deposition levels respond to emission changes. Here, DDM-3D is incorporated into the Urban to Regional Multiscale - One Atmosphere (URM-1ATM) model and is extended to allow speciated aerosol and wet deposition sensitivities to be calculated in addition to ozone and other gas-phase sensitivities. This enhanced version of URM-1ATM produces multidimensional concentration and sensitivity fields that can be used to assess local and regional impacts from individual and distributed sources. In this paper, geographic sensitivity analysis will be used to examine the potential influence of SO_2 emissions from each SAMI state (AL, GA, NC, SC, TN, KY, VA, WV) and areas outside the SAMI region on fine particulate matter (sulfate, nitrate, and ammonium) and sulfate wet deposition levels in the Class I areas in order to make a first-order estimate of the source/receptor relationships.

MODEL DESCRIPTION

The atmospheric modeling system used here consists of the Urban-to-Regional Multiscale - One Atmosphere model (Boylan et al., 2002a; Odman and Russell, 1991a; Kumar et al., 1994) for the air quality modeling, the Regional Atmospheric Modeling System (Pielke et al., 1992) for meteorology, and the Emission Modeling System (Wilkinson et al., 1994) for emissions. The Urban-to-Regional Multiscale - One Atmosphere (URM-1ATM) model is a three-dimensional Eulerian photochemical model that simulates the complex chemical and physical processes that govern the formation, transport, and removal of gas and aerosol-phase pollutants in the atmosphere. The model uses a finite element, variable mesh transport scheme (Odman and Russell, 1991b) and the gas-phase reaction kinetics are calculated using the SAPRC-93 chemical mechanism

(Carter, 1990 and 1995). Secondary particulate matter formation is simulated using ISORROPIA (Nenes et al., 1998), an equilibrium based inorganic aerosol module, and fixed organic aerosol yields (Pandis et al., 1992). The Reactive Scavenging Module (Berkowitz et al., 1989) is used for wet deposition scavenging processes.

Figure 1 shows the domain and grid configuration used by the URM-1ATM model. The grid cell dimensions correspond to 192, 96, 48, 24, and 12 km with the finest resolution (12 km) cells roughly following the southern Appalachian Mountains and the adjacent areas that are expected to most directly influence air quality in the region. Coarser cells are placed in areas that are not expected to contribute as significantly to the air quality problems in the SAM region with the coarsest cells near the boundary of the domain. In the vertical, the domain extends from the surface to a height of 12,867 m above the surface and is divided into seven layers with thickness of 19 m, 43 m, 432 m, 999 m, 1779 m, 3588 m, and 6007 m, respectively. A more detailed discussion on the URM-1ATM model can be found in Boylan et al. (2002a).

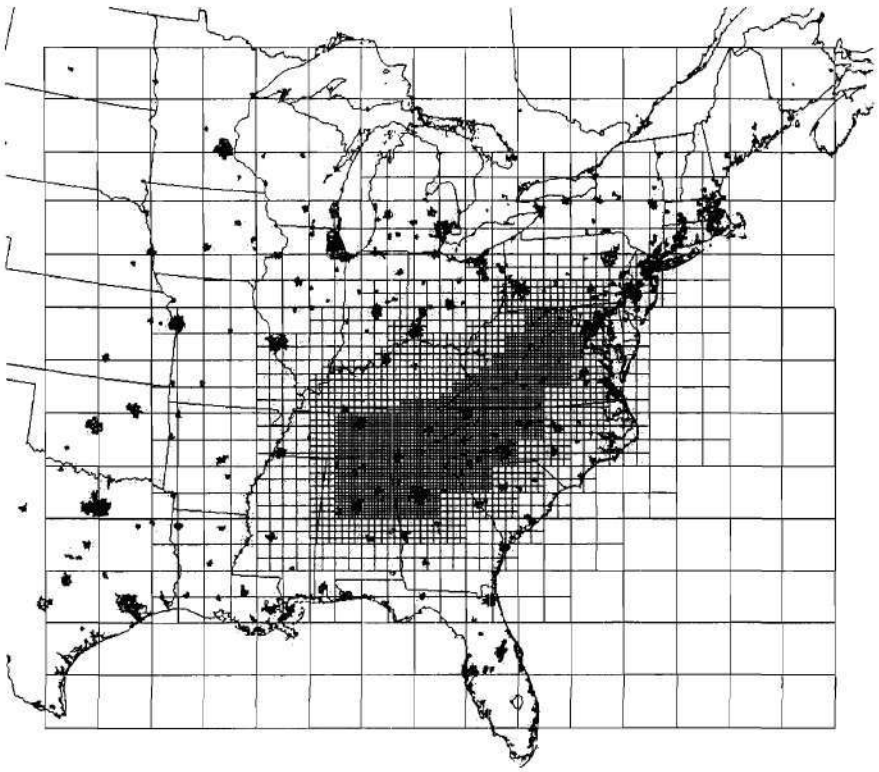

Figure 1: Map of modeling domain and grid structure. The 12-km grid is indicated by the tightly hatched region.

Characterization of the air quality trends requires analysis of data gathered, by either observation or simulation, for several consecutive years. However, modeling several control strategies for multiple years or seasons with the system described above is prohibitive. Because of this limitation, a limited number of episodes that can best represent the five-year running annual average aerosol and acid deposition levels in the Class I areas of the region are used. Using data classification and optimization techniques

(Deuel and Douglas, 1998), nine episodes, each 6 to 9 days long (plus 2 ramp-up days), were selected between the years 1991 and 1995 (Table 1).

Table 1: Episodes used to develop annual aerosol and acid deposition air quality metrics.

Winter Episodes	Spring Episodes	Summer Episodes
February 8-13, 1994	March 23-31, 1993	July 23-31, 1991
	May 11-17,1993	June 24-29, 1992
	April 26-May 3,1995	August 3-11, 1993
	May 24-29, 1995	July 11-19, 1995

The performance of the modeling system has been evaluated by comparing aerosols and acid deposition estimates with the observations for the nine episodes listed in Table 1. For each species contributing to the seasonal and annual metrics, a comprehensive set of statistical calculations has been performed to determine the ability of the model to accurately simulate ambient aerosol concentrations and wet deposition mass fluxes. Aerosol model performance was evaluated by comparing modeling results to observations taken from the Interagency Monitoring of Protected Visual Environments (IMPROVE) monitoring network (NPS, 2000). IMPROVE measurements are taken twice each week and are reported as twenty-four hour average concentrations. Performance statistics were calculated for the thirteen stations in the 12, 24, 48, and 96 km grid cells that IMPROVE measurements were available throughout the episodes. Fine sulfate, ammonium, organics, and $PM_{2.5}$ were biased low and had mean normalized errors of approximately 40 percent. Nitrates were biased high by about 0.5 $\mu g\ m^{-3}$, which might be expected since the IMPROVE filters can be subject to nitrate volatilization. EPA guidance criteria does not exist for determining whether aerosol model performance is acceptable; however, the errors in $PM_{2.5}$ are consistent, if not better, than to those obtained by other models (Seigneur *et al.*, 2001). Wet acid deposition performance was evaluated by comparing modeling results to observations taken from the National Atmospheric Deposition Program (NADP) monitoring network. NADP measurements are taken once each week and the concentrations and precipitation are reported as a seven-day cumulative. Data from the fourteen stations in the 12 km grids were used to determine model performance. Sulfate and nitrate wet deposition were biased low and had mean normalized errors of less than 25 percent. Dry deposition of sulfur and nitrogen were typically over estimated by the model. A detailed evaluation of the performance can be found in Boylan et al. (2002b).

DIRECT SENSITIVITY ANALYSIS

The decoupled direct method for three-dimensional models (DDM-3D) is a sensitivity analysis technique based upon solving a set of equations derived from differentiating the original set of equations governing the atmospheric pollutant dynamics. Using direct

derivatives of the equations governing the evolution of species concentrations, the local sensitivities to a variety of model parameters and inputs are computed simultaneously along with the species concentrations. In equation form, the local sensitivity of a model output (e.g., $PM_{2.5}$ concentration), C_i, to a model input (e.g., emissions) or system parameter (e.g., rate constant), p_j, can be described as:

(1)

Since C is a function of p (the subscripts were dropped for convenience) it can be expanded in a Taylor series for small changes Δp in parameter p around its original value p_0 as:

$$C(p_0 + \Delta p) = C(p_0) + \frac{\partial C}{\partial p}(p_0) \times \Delta p + \frac{\partial^2 C}{\partial p^2}(p_0) \times \Delta p^2 + \cdots . \quad (2)$$

The parentheses in Equation 2 denote functional relationships. As a first order approximation, if the terms with second and higher order derivatives are ignored and the definition of the sensitivity coefficient is used then

$$\Delta C = C(p_0 + \Delta p) - C(p_0) \approx s(p_0) \times \Delta p . \quad (3)$$

Thus, by using the sensitivity coefficient s (i.e., the first derivative of C with respect to p) at $p = p_0$ and Δp, one can estimate ΔC, or the change in C. If C is a linear function of p, then the approximation would be exact for any Δp. Otherwise, Equation 3 is an approximation that is only valid for small Δp. Note that using the higher-order derivatives would yield a more accurate approximation (or similar accuracy for relatively larger Δp). In summary, when using the sensitivity coefficients presented below, keep in mind that the approximation in Equation 3 involves an error. This error would be larger for larger Δp and more nonlinear relationships between C and p.

As developed by Yang et al. (1997), the method takes full advantage of the numerical routines already incorporated into the AQM. Sensitivity coefficients determined by DDM-3D include the response to initial and boundary conditions, horizontal transport, vertical advection and diffusion, emissions, both homogeneous and heterogeneous chemical transformation, aerosol formation, and scavenging processes. The sensitivity coefficients are a function of the concentrations, but the concentrations are not dependent on the sensitivities and can be integrated separately, hence the decoupled nature of the method.

Pollutant sensitivities to the emissions of individual species or lumped species (e.g., NO_x and total VOC) can be calculated. Furthermore, these emissions can be assigned to the entire modeling domain, sub-regions of the domain (e.g., a state or county), or even individual grid cells. The numerical implementation of the sensitivity calculations for transport and gas-phase chemical reaction processes has been extensively documented by Yang et al. (1997) and will not be repeated here. Only the calculation of sensitivity coefficients for aerosols and wet deposition will be discussed.

The aerosol module (Ansari and Pandis, 1999) embedded into URM-1ATM has the capability of treating explicitly all major components of primary and secondary PM. The continuous aerosol size distribution is modeled following a sectional approach (i.e., discrete size bins are specified for particles with diameters inside a given range). The particles within each size bin are assumed to have the same composition. Here, four size bins are specified: smaller than 0.156 μm, 0.156-0.625 μm, 0.625-2.5 μm and 2.5-10 μm, though the number and bin boundaries can be changed to suit the specific application. Thus, adding the first three size bins gives the $PM_{2.5}$ concentration (or sensitivity), while the sum of all four size bins yields the PM_{10} concentration (or sensitivity). Particles larger than PM_{10} are assumed to have a short lifetime in the atmosphere (i.e., they deposit rapidly) so they are not modeled here. The selection of four size bins is a trade-off between accuracy in simulating the PM dynamics and computational resources.

Due to the existence of different chemical components of real aerosols, modeled aerosol species have been divided into three groups: inorganic equilibrium species, organic species and non-reactive species. Inorganic aerosol species that are modeled include ammonium, nitrate, sulfate, sodium, chloride, and hydrogen ion. The thermodynamic equilibrium between the gas-, liquid- and particulate-phase of the inorganic aerosol species is simulated with ISORROPIA (Nenes et al., 1998). ISORROPIA is a computationally efficient and rigorous model that calculates the state and composition of the inorganic fraction of the aerosol. The 15 equilibrium reactions that are solved by ISORROPIA are listed in Table 2. The organic fraction of the aerosols is represented as a single lumped species, which is computed as the sum of all semi-volatile organic compounds that are either emitted or produced from the gas-phase oxidation of organic gases and condensed to the particulate phase. The production of condensable organics from atmospheric oxidation of VOCs is based on the yields of Pandis et al. (1992). To derive the amount of condensation/volatilization affecting the particles of each size bin, the interaction between the gas-phase and the particles in the different size bins is modeled using a mass transfer algorithm (Pandis et al., 1993). The effects of nucleation and coagulation are neglected. Lastly, the inert fraction of the aerosol, which undergoes transport, growth, and deposition includes: calcium, elemental carbon (EC), magnesium, potassium, and a lumped category that incorporates all other inert PM species.

Table 2: Equilibrium relations and equilibrium constant expressions solved by ISORROPIA.[a]

Reaction	Equilibrium constant expression (K_m)
$H_2O_{(aq)} \xleftrightarrow{K_w} H^+_{(aq)} + OH^-_{(aq)}$	$\left([H^+][OH^-] / a_w \right) \cdot \gamma_{H^+}\gamma_{OH^-}$

$HSO_{4(aq)}^{-} \xleftrightarrow{K_1} H_{(aq)}^{+} + SO_{4(aq)}^{2-}$	$\frac{[H^+][SO_4^{2-}]}{[HSO_4^-]} \frac{\gamma_{H^+}\gamma_{SO_4^{2-}}}{\gamma_{HSO_4^-}}$
$NH_{3(g)} \xleftrightarrow{K_{2a}} NH_{3(aq)}$	$\left([NH_3] / P_{NH_3} \right) \cdot \gamma_{NH_3}$
$NH_{3(aq)} + H_2O_{(aq)} \xleftrightarrow{K_{2b}} NH_{4(aq)}^{+} + OH_{(aq)}^{-}$	$\frac{[NH_4^+][OH^-]}{[NH_{3(aq)}]a_w} \frac{\gamma_{NH_4^+}\gamma_{OH^-}}{\gamma_{NH_3}}$
$HCl_{(g)} \xleftrightarrow{K_3} H_{(aq)}^{+} + Cl_{(aq)}^{-}$	$\left([H^+][Cl^-] / P_{HCl} \right) \cdot \gamma_{H^+}\gamma_{Cl^-}$
$HNO_{3(g)} \xleftrightarrow{K_4} H_{(aq)}^{+} + NO_{3(aq)}^{-}$	$\left([H^+][NO_3^-] / P_{HNO_3} \right) \cdot \gamma_{H^+}\gamma_{NO_3^-}$
$Na_2SO_{4(s)} \xleftrightarrow{K_5} 2Na_{(aq)}^{+} + SO_{4(aq)}^{2-}$	$[Na^+]^2[SO_4^{2-}]\gamma_{Na^+}^2\gamma_{SO_4^{2-}}$
$NH_4Cl_{(s)} \xleftrightarrow{K_6} NH_{3(g)} + HCl_{(g)}$	$P_{NH_3}P_{HCl}$
$(NH_4)_2SO_{4(s)} \xleftrightarrow{K_7} 2NH_{4(aq)}^{+} + SO_{4(aq)}^{2-}$	$[NH_4^+]^2[SO_4^{2-}]\gamma_{NH_4^+}^2\gamma_{SO_4^{2-}}$
$NaCl_{(s)} \xleftrightarrow{K_8} Na_{(aq)}^{+} + Cl_{(aq)}^{-}$	$[Na^+][Cl^-]\gamma_{Na^+}\gamma_{Cl^-}$
$NaNO_{3(s)} \xleftrightarrow{K_9} Na_{(aq)}^{+} + NO_{3(aq)}^{-}$	$[Na^+][NO_3^-]\gamma_{Na^+}\gamma_{NO_3^-}$
$NH_4NO_{3(s)} \xleftrightarrow{K_{10}} NH_{3(g)} + HNO_{3(g)}$	$P_{NH_3}P_{HNO_3}$
$NaHSO_{4(s)} \xleftrightarrow{K_{11}} Na_{(aq)}^{+} + HSO_{4(aq)}^{-}$	$[Na^+][HSO_4^-]\gamma_{Na^+}\gamma_{HSO_4^-}$
$NH_4HSO_{4(s)} \xleftrightarrow{K_{12}} NH_{4(aq)}^{+} + HSO_{4(aq)}^{-}$	$[NH_4^+][HSO_4^-]\gamma_{NH_4^+}\gamma_{HSO_4^-}$
$(NH_4)_3H(SO_4)_{2(s)} \xleftrightarrow{K_{13}}$ $3NH_{4(aq)}^{+} + HSO_{4(aq)}^{-} + SO_{4(aq)}^{2-}$	$[NH_4^+]^3[SO_4^{2-}][HSO_4^-] \cdot \gamma_{NH_4^+}^3\gamma_{SO_4^{2-}}\gamma_{HSO_4^-}$

[a] Nomenclature details: a_w is water's activity, γ_i is the activity coefficient of species i, $[i]$ is the concentration of species i, K_m is the equilibrium constant for reaction m, P_i is the partial pressure of species i.

Aerosol sensitivities for the inorganic equilibrium species are calculated in two steps. The first involves the condensation and evaporation of gas and aerosol species, while the second step involves the growth of particles in each aerosol size bin. The derivative of each equilibrium equation in Table 2 is calculated to produce 15 sensitivity expressions. For example, the derivative of the sulfate concentration with respect to parameter p_j for the second equilibrium expression in Table 2, i.e.,

$$[SO_4^{2-}] = \frac{K_1 \gamma_{HSO_4^-}}{\gamma_{H^+}\gamma_{SO_4^{2-}}} \frac{[HSO_4^-]}{[H^+]} \tag{4}$$

would yield:

$$\frac{\partial[SO_4^{2-}]}{\partial p_j} = [SO_4^{2-}]\left(\frac{-1}{[H^+]}\frac{\partial[H^+]}{\partial p_j} + \frac{1}{[HSO_4^-]}\frac{\partial[HSO_4^-]}{\partial p_j} + \frac{\gamma_{H^+}\gamma_{SO_4^{2-}}}{\gamma_{HSO_4^-}}\frac{\partial}{\partial p_j}\left(\frac{\gamma_{HSO_4^-}}{\gamma_{H^+}\gamma_{SO_4^{2-}}} \right) \right) \tag{5}$$

Functionally, the last term involving the activities is complex. However, the activities are constrained by the relative humidity, reducing the sensitivity to other parameters. Since the relative humidity does not change with p_j, this last term is neglected.

To complete the set of sensitivity equations, the derivative of the mass conservation and charge balance expressions are required. Table 3 shows the mass conservation and the charge balance expressions (12 expressions). For example, the derivative of the total nitrate (TN) expression yields:

$$\frac{\partial[TN]}{\partial p_j} = \frac{\partial[AN]}{\partial p_j} + \frac{\partial[HNO_3]}{\partial p_j} \tag{6}$$

where, $[TN]$ is the total nitrate concentration, $[AN]$ is aerosol nitrate concentration, and $[HNO_3]$ is the nitric acid concentration. The resulting 27 (=15+12) sensitivity equations are solved simultaneously to produce the desired sensitivities for aerosol sulfate, nitrate, ammonium, sodium, chloride and hydrogen, in addition to the sensitivities for gas-phase HNO_3, NH_3 and HCl.

Because the production of condensable organics is calculated in the gas-phase module of URM-1ATM, the sensitivity coefficients for the organic aerosols are computed in the same way as the gas-phase species. However, extension to using more thermodynamically comprehensive models for semi-volatile organic PM (e.g. using partitioning coefficients) is straight forward. Finally, the sensitivities for the aerosol species are apportioned to each size bin according to the individual species' concentration in each size bin.

Table 3: Mass conservation and charge balance expressions.[a]

$$[TS] = [AS]$$
$$[TN] = [AN] + [HNO_3]$$
$$[TA] = [AA] + [NH_3]$$
$$[TNa] = [ANa]$$
$$[TCl] = [ACl] + [HCl]$$
$$[AS] = [SO_4^{2-}] + [HSO_4^-] + [NaHSO_4] + [NH_4HSO_4] + [Na_2SO_4] + [(NH_4)_2SO_4] + 2[(NH_4)_3H(SO_4)_2]$$
$$[AN] = [NO_3^-] + [HSO_4^-] + [NaNO_3] + [NH_4NO_3]$$
$$[AA] = [NH_4^+] + [HSO_4^-] + [NH_4NO_3] + [NH_4HSO_4] + [NH_4Cl] + 2[(NH_4)_2SO_4] + 3[(NH_4)_3H(SO_4)_2]$$
$$[ANa] = [Na^+] + [HSO_4^-] + [NaHSO_4] + [NaNO_3] + 2[Na_2SO_4] + [NaCl]$$
$$[ACl] = [Cl^-] + [NH_4Cl] + [NaCl]$$
$$[AH] = 2[AS] + [AN] + [ACl] - [AA] - [ANa]$$
$$[H^+] = 2[SO_4^{2-}] + [HSO_4^-] + [NO_3^-] + [Cl^-] + [OH^-] - [NH_4^+] - [Na^+]$$

[a]Definition of abbreviations: TS = total sulfate, TN = total nitrate, TA = total ammonium, TNa = total sodium, TCl = total chloride, AS = aerosol sulfate, AN = aerosol nitrate, AA = aerosol ammonium, ANa = aerosol sodium, ACl = aerosol chloride, AH = aerosol hydrogen.

Next, the "growth" of aerosol sensitivities is calculated using the aerosol droplet currents (Friedlander, 1977). The aerosol droplet current can be represented by:

$$\frac{\partial M}{\partial t} = -\frac{\partial (mI)}{\partial V} + \rho I \tag{7}$$

where M is the aerosol mass distribution function ($\mu g\ m^{-3}$), I is the particle current (number of particles per unit time; sec^{-1}), m is the particle mass (μg), V is the particle volume (m^{-3}), and ρ is the particle density ($\mu g\ m^{-3}$). The particle current calculated from the aerosol growth module is used to "grow" the sensitivity coefficients through the particle space. Taking the derivative of Equation 7 results in:

$$\frac{\partial}{\partial t}\left(\frac{\partial M}{\partial p_j}\right) = -\frac{\partial}{\partial V}\left(m\frac{\partial I}{\partial p_j}\right) + \rho\frac{\partial I}{\partial p_j} \tag{8}$$

This sensitivity equation is solved for each size bin assuming that growth sensitivity by size is proportional to the original growth distribution, along with a stability criterion to produce the sensitivity coefficients for particle growth. The stability criteria is:

$$\Delta t \leq \frac{1}{I} \tag{9}$$

where, Δt is the integration time step. The total aerosol sensitivity results for each species in each size bin are then determined by allowing the sensitivity coefficients to be updated by both the condensation/evaporation and particle growth sensitivity calculations.

The gas and aerosol sensitivities are impacted by wet deposition and scavenging processes that are simulated by the Reactive Scavenging Module (Berkowitz et al., 1989). Column mass fluxes before (o) and after (t) RSM are calculated and used to scale the sensitivity coefficients for each species:

$$s_k^t = \frac{\sum_{k=1}^{l}\left(c_k^t\right)\left(\Delta z_k\right)}{\sum_{k=1}^{l}\left(c_k^o\right)\left(\Delta z_k\right)} s_k^o \tag{10}$$

where, s_k and c_k are the sensitivities and concentrations at layer k, l is the number of layers, and Δz_k is the thickness of layer k. The wet deposition mass flux sensitivity (S_{wet}) for each species is calculated as:

$$S_{wet} = \sum_{k=1}^{l}\left(s_k^o\right)\left(\Delta z_k\right) - \sum_{k=1}^{l}\left(s_k^t\right)\left(\Delta z_k\right) \tag{11}$$

Combining the sensitivity calculations from each module results in a set of integrated sensitivity coefficients. The sensitivity coefficients for the gas and aerosol species are in units of ppm and $\mu g\ m^{-3}$ per percent increase in the parameter of interest (e.g. 10% increase in NO_x emissions), respectively. The wet deposition sensitivity coefficients are in units of $mg\ m^{-2}$ per percent increase in the parameter of interest.

Comparison of DDM-3D and Brute Force Methods

A "brute-force" approach has been traditionally used to calculate the response of a model to changes in various input parameters. This method involves running the model a number of different times, each time perturbing one parameter and comparing the results to the basecase run. The brute force approach has been used extensively to study the response of ozone (e.g. McNair et al.,1992; Winner et al.,1995; Bergin et al., 1998) and $PM_{2.5}$ (e.g. Seigneur et al., 2000) in air quality models to various model inputs including emissions. However, if the perturbation is small, the brute-force method may not yield accurate sensitivities due to numerical errors propagated in the model. Most of the time, the response of the models to small perturbations would be within the error bounds of the basecase estimates. Moreover, as the number of perturbed parameters increases, the feasibility of the approach is hampered by computational resource limitations. On the other hand, the DDM-3D technique uses direct derivatives of the governing equations and allows the user to perform numerous sensitivity calculations in a single model run.

The sensitivity is defined as the first derivative with respect to the parameter (i.e., response to an infinitesimal change in the parameter); therefore, DDM-3D is, by definition, most accurate for small perturbations. However, DDM-3D has the disadvantage of only providing first-order sensitivity coefficients; inaccurate sensitivities may result for large changes in independent variables if the response is non-linear.

Both DDM-3D and the brute force sensitivity techniques were applied to the SAM modeling domain for the July 11-19, 1995 episode using emissions for the year 2010. A comparison was made for the sensitivity coefficients produced for each aerosol component and each wet deposition species to emissions of SO_2, NO_x, VOCs, and NH_3. In this paper, we concentrate on the sensitivity of aerosols (sulfate, nitrate, ammonium, and $PM_{2.5}$) and sulfate wet deposition to changes in SO_2 emissions. Other species such as ozone, organic and non-reactive aerosols, and nitrate and ammonium wet deposition show little sensitivity to SO_2 emissions and will not be discussed.

Figure 2 shows a comparison of aerosol sulfate sensitivities to a 30% reduction in domain-wide SO_2 emissions using DDM-3D and the brute force techniques. The results shown are 24-hour averaged sensitivities for July 15. Both methods show a reduction in sulfate concentrations in the SAM region ranging from approximately 1.2 – 4.7 $\mu g\ m^{-3}$ and very similar spatial patterns. Also shown in the figure are the values for the minimum and maximum sensitivities along with their respective grid locations. The nitrate, ammonium, and $PM_{2.5}$ aerosol sensitivities obtained from DDM-3D also match well with the brute force results (not shown).

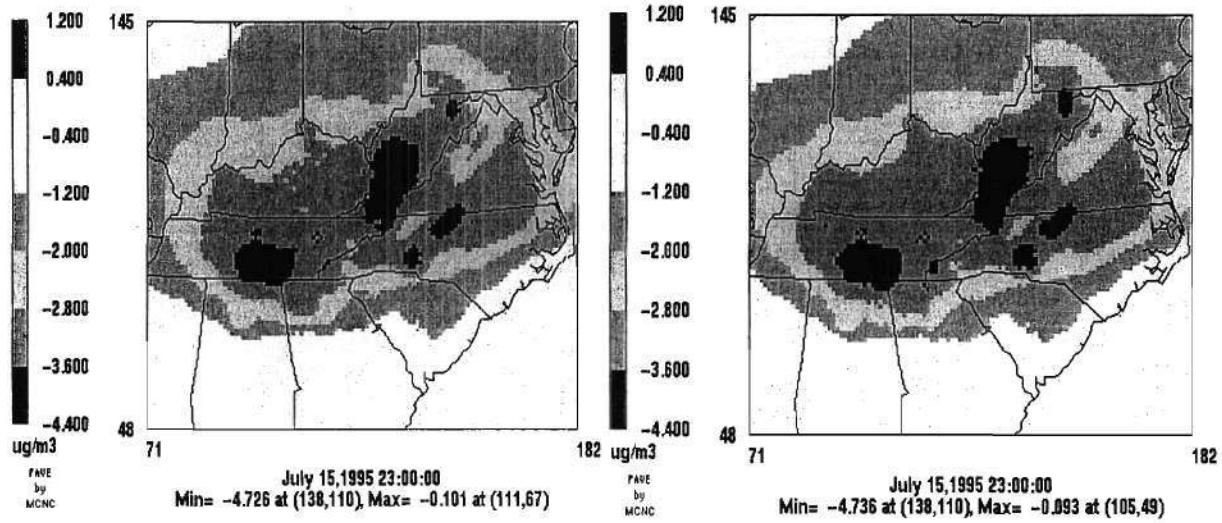

Figure 2: Sulfate aerosol sensitivities to 30% reduction in SO_2 emissions using DDM-3D (left) and brute force (right).

Figure 3 shows a comparison of sulfate wet deposition sensitivities to a 30% reduction in domain-wide SO_2 emissions using DDM-3D and the brute force techniques. The results are 7-day cumulative sensitivities for the week of July 11-18. Both methods show reductions in sulfate wet deposition of up to 60 mg m^{-2} and very similar spatial patterns. Nitrate and ammonium wet deposition sensitivities to changes in SO_2 emissions were very small.

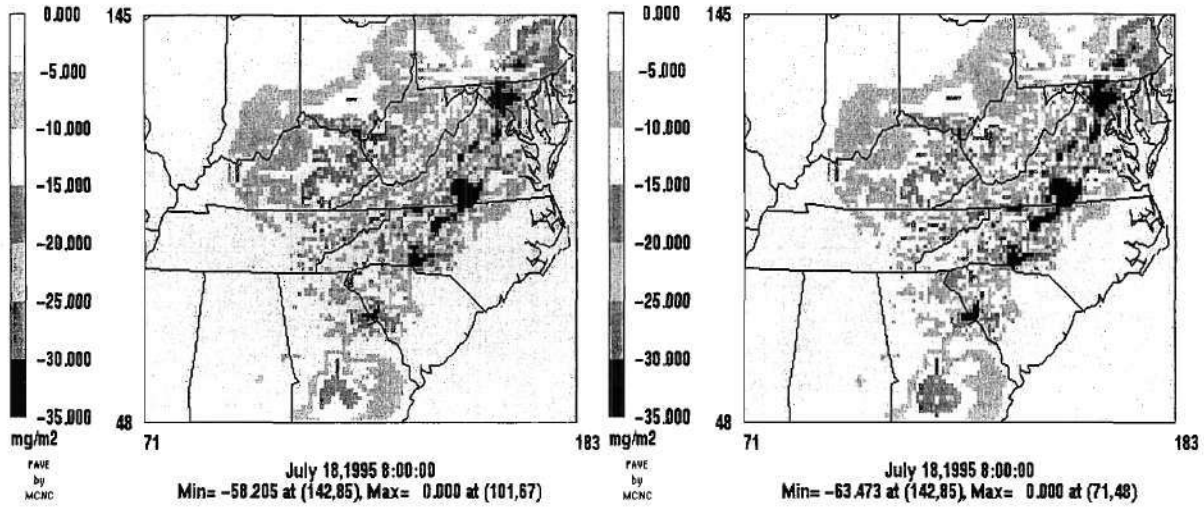

Figure 3: Sulfate wet deposition sensitivities to 30% reduction in SO_2 emissions using DDM-3D (left) and brute force (right).

Both the DDM-3D and brute force methods provide nearly identical results. However, in the time it took to produce the basecase and one sensitivity run using the brute force method, a basecase and thirteen sensitivities were produced using the DDM-3D technique.

METHODOLOGY FOR ANNUAL AVERAGE POLLUTANT SENSITIVITIES

Nine multi-day episodes (Table 1) were modeled to represent the full spectrum of ozone, deposition, and visibility under a variety of conditions (Boylan et al., 2002b and 2002c). Episodic model results can be scaled up to estimate annual average pollutant levels. SAMI categorized week-long acid deposition periods into one of four classes (1-4). The class varied with the observed total mass of selected cations and anions (sulfate, nitrate, Ca and Mg) in precipitation. Assignment to one of the five visibility classes was determined using measured total fine aerosol mass. In each case, class number increased with the severity of pollutant levels with Class 1 days being the least polluted and Class 4 and 5 days being the most polluted. Table 4 shows the percentage of days each year that are represented by each class. All classes were defined based on data at two national parks, Great Smoky Mountains (GRSM) in Tennessee/North Carolina and Shenandoah (SHEN) in Virginia.

Table 4: Percent of days falling into each Class

Species	Class 1	Class 2	Class 3	Class 4	Class 5
Wet Deposition	70%	20%	7%	3%	N/A
Visibility	20%	30%	30%	17%	3%

Table 5 lists all of the modeled days for which there were IMPROVE aerosol observations, the assigned visibility class, and the percentage contribution to the annual visibility metrics at the GRSM and SHEN National Parks. Table 6 lists the week-long periods for which there were NADP wet deposition observations. Also included are the assigned classes and the percentage contribution to the annual wet deposition metrics at GRSM and SHEN. For a more detailed discussion on episode selection and classification, refer to Deuel and Douglas (1998).

Table 5: Aerosol classes and their contribution to the annual visibility metric.

Date	GRSM		SHEN	
(MM/DD/YY)	Class	Weight (%)	Class	Weight (%)
07/24/91	-	-	4	2.10
07/27/91	5	1.39	-	-
07/31/91	5	0.38	4	2.19
06/24/92	4	4.03	4	0.79
06/27/92	-	-	4	0.79
03/24/93	2	26.41	2	1.37
03/27/93	1	10.39	-	-
03/31/93	-	-	1	17.90
05/12/93	-	-	4	2.55
05/15/93	3	6.99	3	4.50
08/04/93	3	4.60	3	2.95
08/07/93	3	4.60	4	2.55
08/11/93	4	4.03	4	1.58
02/09/94	1	14.98	1	17.90
04/26/95	2	3.59	2	10.14
04/29/95	3	9.16	2	10.14
05/03/95	-	-	2	10.14
05/24/95	-	-	4	2.10
05/27/95	4	4.03	3	3.26
07/12/95	4	4.03	5	2.05
07/15/95	5	1.39	5	2.05
07/19/95	-	-	3	2.95

Table 6: Wet Deposition Classes and Weights

Period	GRSM		SHEN	
(MM/DD/YY)	Class	Weight (%)	Class	Weight (%)
07/23/91 – 07/30/91	4	3.81	4	2.00
06/23/92 – 06/30/92	2	18.36	1	30.79
03/23/93 – 03/30/93	2	9.13	3	13.88
05/11/93 – 05/18/93	3	4.46	4	2.00
08/03/93 – 08/10/93	3	4.46	-	-
02/08/94 – 02/15/94	2	9.13	2	4.75
04/25/95 – 05/01/95	1	14.61	2	11.05
05/23/95 – 05/30/95	1	36.04	2	4.75
07/11/95 – 07/18/95	-	-	1	30.79

The annual average pollutant level and annual average sensitivity at each site is calculated as:

$$C_{average} = \frac{\sum_{i=1}^{N} w_i C_i}{\sum_{i=1}^{N} w_i} \tag{12}$$

$$S_{average} = \frac{\sum_{i=1}^{N} w_i S_i}{\sum_{i=1}^{N} w_i} \tag{13}$$

where, $C_{average}$ and $S_{average}$ are the annual average pollutant levels and sensitivities, N is the number of days or periods contributing to the metric, w_i is the percent contribution or weight (from Tables 5 and 6) to the annual metric, and C_i and S_i are the weighted pollutant levels and sensitivities for individual periods (days or weeks). When the annual average is calculated using the weights and modeling results for all time periods contributing to the annual average, the Σw_i term will be 100%. However, if pollutant levels and sensitivities are calculated by individual class, the Σw_i term will be less than 100% and is used to normalize each class to its average value.

Annual weights are only defined at two sites (GRSM and SHEN). However, these weights are applied to calculate annual average PM and deposition at other Class I areas by assuming that sites south of Virginia and Kentucky are represented by the weights at GRSM and sites north of North Carolina and Tennessee are represented by the SHEN weights.

APPLICATION TO THE SOUTHERN APPALACHIAN MOUNTAINS

Sensitivity analysis has been performed for the nine episodes using emissions estimated for the year 2010 and meteorological data from each 1991 – 1995 basecase episode. The year 2010 was chosen because the sensitivity results were initially to be used by SAMI to guide the design of control strategies. In the end, the results were used to provide information on relative impact of different geographic regions on Class I areas. The 2010 emission estimates assume reductions of volatile organic compounds (VOCs) and oxides of nitrogen (NO_x) emissions from the laws and regulations mandated by the Clean Air Act (CAA) as amended in 1977 and 1990 to comply with the 1-hour ozone standard; reductions of SO_2 and NO_x from utility sources under Title IV of the CAA amendments; and reductions of NO_x and VOCs from mobile sources under Tier I tailpipe standards and fuel rules. In addition, emission reductions are assumed from several

recently promulgated regulations: regional NO_x reductions which will be included in "State Implementation Plans" to reduce ozone (USEPA, 1998); NO_x and VOC reductions resulting from implementation of Tier II and low sulfur rules (USEPA, 2001); and VOC reductions resulting from Maximum Achievable Control Technology (MACT) standards (USEPA, 1990). Emission reductions that might be required for the 8-hour ozone National Ambient Air Quality Standards (NAAQS), the new $PM_{2.5}$ NAAQS, or the regional haze rule are not included. For a more complete description, refer to Pechan (2001).

For this study, the domain was divided into 13 sub-domains and the responses of $PM_{2.5}$ and sulfate wet deposition levels to emissions from each sub-domain were estimated. The regional sub-domains are listed in Table 7. Each of the eight SAM states is treated as an individual sub-domain. The other 5 sub-domains consist of the Midwest, Northeast, Central, Florida/Mississippi, and a region that contains all other emissions not represented by the other 12 sub-domains. Table 8 contains the sites in the Appalachian Mountains where aerosol and sulfate wet deposition sensitivities were evaluated. Figure 4 shows the geographic location of each receptor site (SAMI, 2001).

Table 7: List of states in each source region used for sensitivity analysis.

Region	States
SAMI	Alabama (AL), Georgia (GA), South Carolina (SC), North Carolina (NC), Tennessee (TN), Kentucky (KY), Virginia (VA), West Virginia (WV)
Midwest (MW)	Ohio, Michigan, Indiana, Illinois, Wisconsin
Northeast (NE)	Maryland, Delaware, District of Columbia, Pennsylvania, New Jersey, New York, Connecticut, Massachusetts, Rhode Island, Vermont, New Hampshire, Maine
Central (CN)	Louisiana, Arkansas, Missouri, Iowa, Minnesota[a], Texas[a], Oklahoma[a], Kansas[a], Nebraska[a]
Florida/Mississippi (FM)	Florida[a], Mississippi
All Others (AO)	South Dakota[a], North Dakota[a], Canada, Major Bodies of Water

[a]Entire state is not contained in the modeling domain

Table 8: Labels, and locations for receptors in Class I national parks and wilderness areas used in sensitivity analysis.

Site Name	Label	State
Sipsey	SIPS	AL
Cohutta	COHU	GA
Joyce Kilmer	JOKM	NC
Look Rock[a], Great Smoky Mountains	GRSM	TN
Elkmont[b], Great Smoky Mountains	ELKM	TN
Clingmans Dome[b], Great Smoky Mountains	CLND	TN
Shining Rock	SHRO	NC

Linville Gorge	LIGO	NC
Jefferson/James River Face	JEFF	VA
Shenandoah	SHEN	VA
Otter Creek	OTRC	WV
Dolly Sodds	DOSO	WV

[a]Location of the IMPROVE monitor in the Great Smoky Mountains. This site will only be used to look at aerosol sensitivities.

[b]These sites are located in the Great Smoky Mountains and will only be used to look at sulfate wet deposition sensitivities. ELKM is a low elevation site and CLND is a high elevation site.

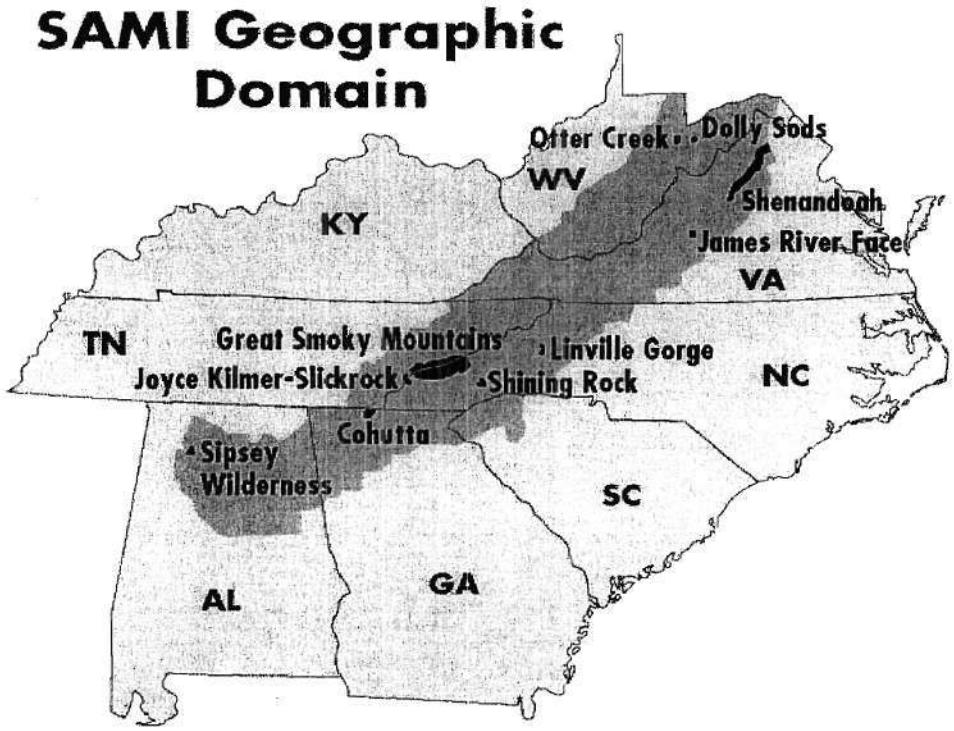

Figure 4: Geographic location of the Class I receptor sites where sensitivity analysis was performed (SAMI, 2001).

Recall from Figure 1 that the grid resolution coarsened outside the SAMI states. There were very few fine cells where the Northeast region borders the SAMI states. In general, grid-cell sizes over the regional sub-domains were 48-km or larger. Among all regional sub-domains, the Central region was modeled using the largest cell sizes. Large grid sizes dilute emissions by instantaneous mixing of plumes inside the grid cell leading, in general, to higher local concentrations of secondary pollutants and less transport of precursors. Because of this grid-resolution issue, the most reliable source-receptor relationships are likely those originating from the SAM region and ending in the SAMI region, followed by those originating from the SAMI region and ending in the regional

sub-domains. The least accurate would be the source-receptor relationships originating from the regional sub-domains and ending in the SAMI states. Since no special point-source treatment was used in this study, the impact of point-source plumes originating from regional sub-domains may be highly inaccurate. For example, elevated SO_2 and NO_x sources in the Central region may actually have a larger impact on sulfate and ozone concentrations at the receptors within the SAMI region than what is projected here.

For small perturbations, one can assume linearity and use the DDM sensitivities in combination. For example, the sensitivities to emissions from 8 SAMI states were added to find the sensitivity to emissions from the SAMI region. Similarly, the sensitivities to emissions from the six regions in Table 7 were added to find the sensitivity to domain-wide emissions. The sensitivities to different source types can also be added. For example, the sensitivities of ozone to elevated and ground-level NO_x sources can be added to find the sensitivity to total NO_x sources. It is also possible to calculate more complex combinations such as the sensitivity of fine sulfate aerosol to multiple emission types (e.g., SO_2, NO_x, NH_3) from different states and regions. However, the result would be valid only if the linearity assumption still holds under the selected combination. Providing validity bounds for the linearity assumption is beyond the scope of this paper. Note that large or combinatory emission perturbations would eventually lead to nonlinearities at which point the DDM results would cease to be reliable. Here, after some limited comparisons with the "brute-force" method, DDM results were scaled and presented for a 10% reduction in SO_2 emissions. Although the results presented below are for a 10% reduction in SO_2 emissions, it was shown earlier that the response is linear up to at least a 30% reduction in SO_2 emissions. The sensitivity results here should not be used as a replacement for full-scale modeling in evaluating the effectiveness of a control strategy.

Aerosol Sensitivity Results

Hourly and daily sensitivity coefficients were computed for each grid cell in the domain for the year 2010. The sensitivity of regional daily average $PM_{2.5}$ concentrations to a 10% reduction in total (elevated plus ground-level) SO_2 emissions from each of the eight SAMI states and surrounding regions was mapped for each day contributing to the annual metric (i.e., IMPROVE days). Figure 5 shows the modeled daily average $PM_{2.5}$ concentration (first frame in second row) and the absolute change in concentration due to a 10% reduction in SO_2 emissions from each of the SAMI states on July 15, 1995 (using 2010 emissions). On this particular day, the impact of emission reductions from many states are local except for Alabama and Georgia whose reductions benefit the neighboring states to the northwest. This is, in part, due to a high pressure system over the SAMI region and the anti-cyclonic wind patterns around it.

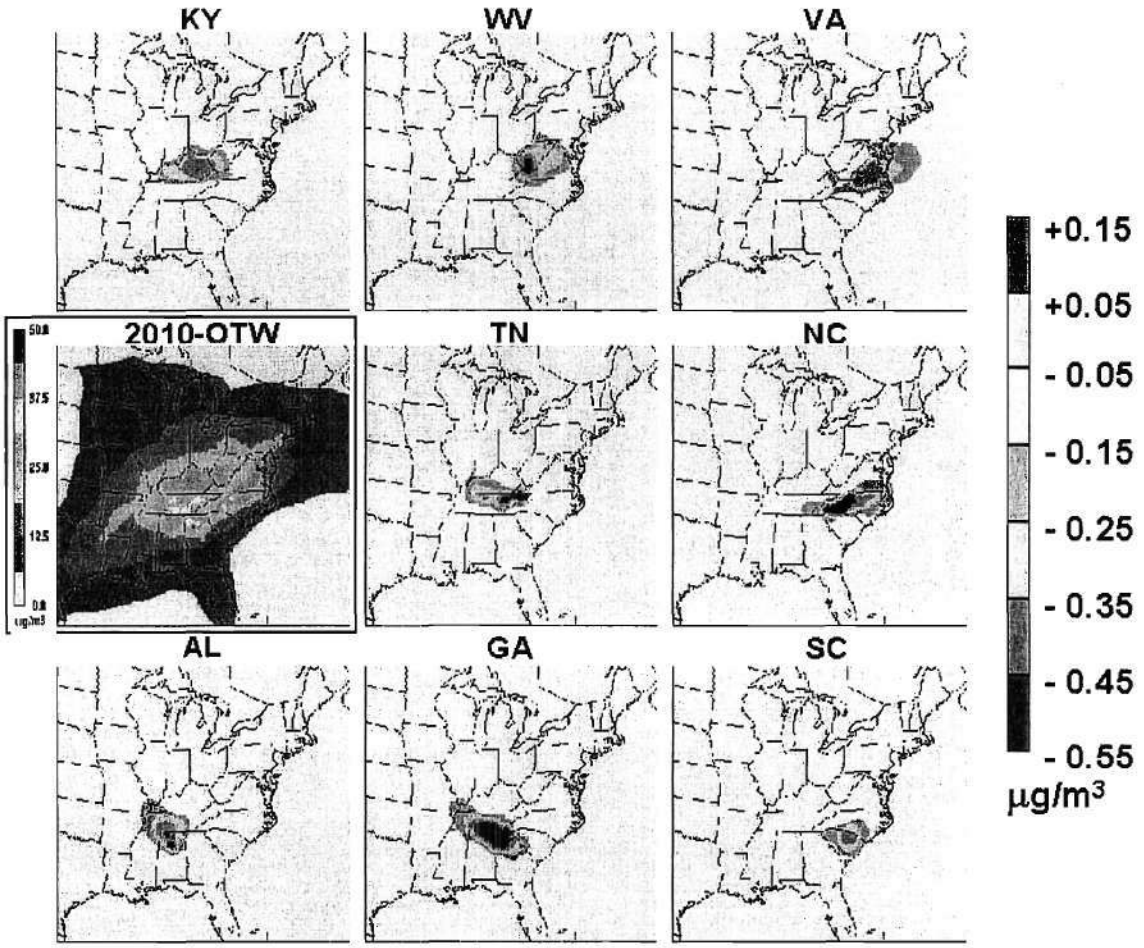

Figure 5: Daily average $PM_{2.5}$ and its change on July 15, 1995 (using 2010 emissions) for a 10% reduction in SO_2 emissions from the SAMI states.

By examining sensitivities at a specific station, it is possible to determine the sub-domain from which emission reductions would have the greatest effect. Specifically, this discussion will focus on the sensitivity of fine sulfate, nitrate, ammonium, and $PM_{2.5}$ at the ten Class I sites listed in Table 8 to SO_2 emission reductions from the thirteen regions listed in Table 7. Figure 6 shows the daily averaged sulfate concentrations (right y-axis) and sensitivities (left y-axis) for each weighted IMPROVE day at GRSM. The sulfate sensitivities represent the percent change in sulfate concentrations due to a 10% SO_2 emission reduction from each geographic sub-domain. The modeled concentrations are included to give the reader an idea as to the magnitude of the absolute sulfate concentration change (percent change multiplied by the sulfate concentration) and allows the significance of the reductions to be evaluated against the total $PM_{2.5}$ concentrations. Since the sensitivity of each sub-domain can be viewed as a contribution to the sum, the sensitivity to a 10% domain-wide emission reduction can be calculated by summing the sensitivities for each of the sub-domains, assuming the response is linear. For example, if the meteorology of July 15, 1995 reoccurs in 2010, a 10% reduction in domain-wide SO_2

emissions is estimated to result in an 8.8% reduction in the sulfate concentration at GRSM. Of this, 2.8% is connected to TN, 1.5% to GA, 1.2% to NC, and smaller fractions to the other 10 sub-domains assuming they all reduced their SO_2 emissions by 10%. At GRSM, it can be seen that different sub-domains can have varying contributions to the overall reduction of sulfate from day-to-day depending on the specific meteorology.

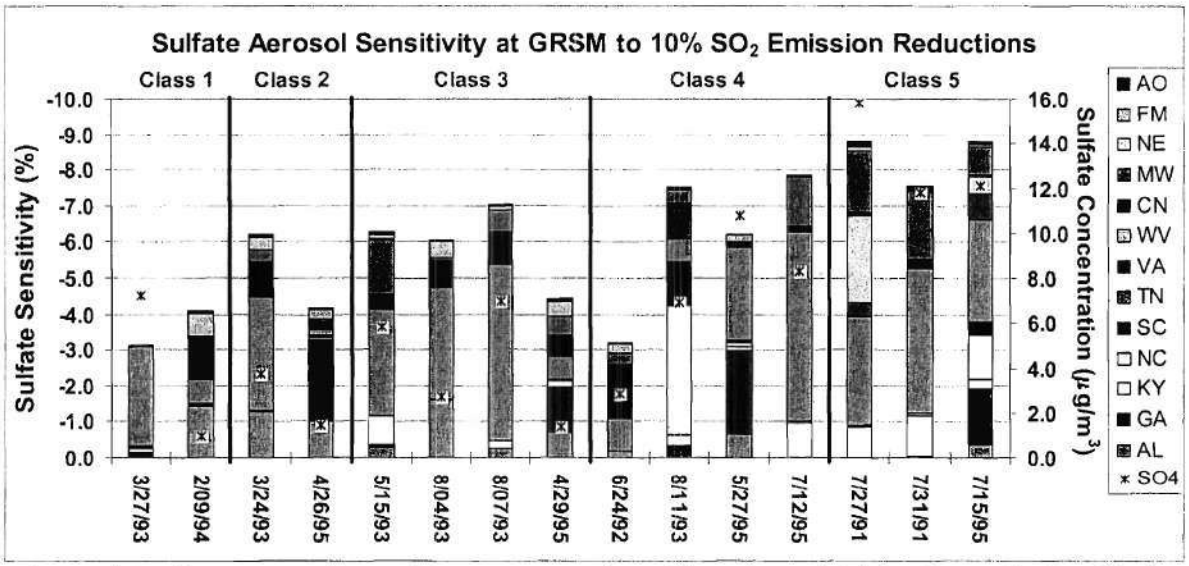

Figure 6: Daily average fine sulfate concentrations (*) and sensitivities for each classified day at Great Smoky Mountains to a 10% reduction in SO_2 emissions from each geographic sub-domain.

Figure 7 contains the annual average and class average sulfate concentrations and sensitivity contributions to sulfate reductions at GRSM. The contribution from TN is somewhat constant across classes, but the sensitivity to domain-wide reductions vary depending on the roles of the other 12 sub-domains. It is clear that there are greater responses to SO_2 emission reductions on days with the highest pollutant concentrations (Class 4 and 5 days), both in an absolute and relative sense.

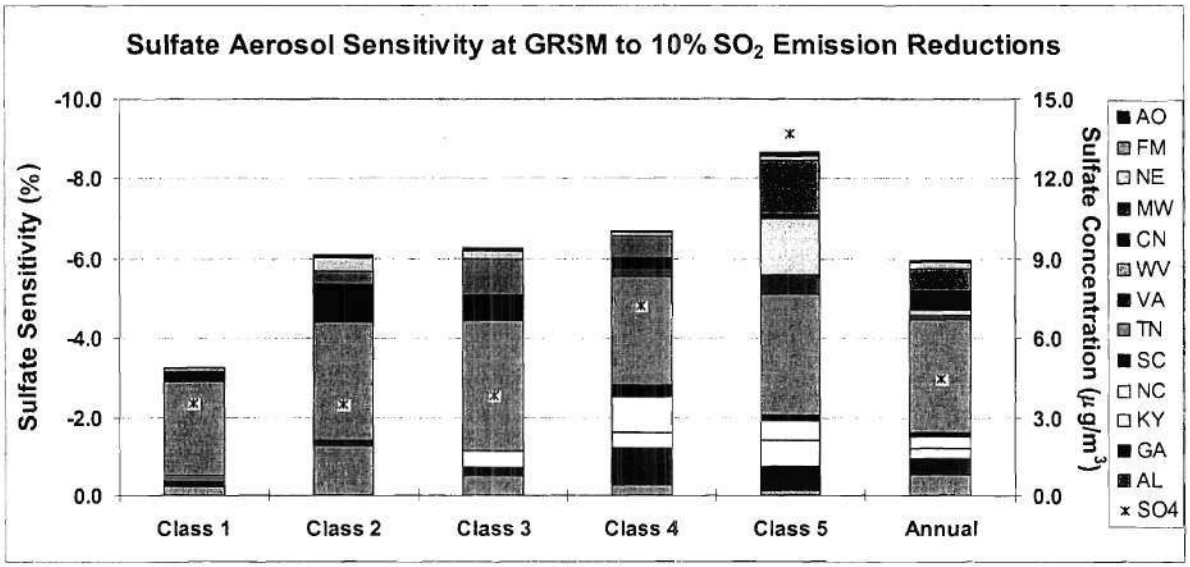

Figure 7: Daily average fine sulfate concentrations (*) and sensitivities for each class at Great Smoky Mountains to a 10% reduction in SO_2 emissions from each geographic sub-domain.

Figure 8 contains the annual average fine sulfate concentrations and sensitivities for ten Class I areas to a 10% reduction in SO_2 emissions from different sub-domains. The stations are geographically ordered from southwest to northeast. The sites in Alabama and Georgia (SIPS, COHU) show high responses to emission reductions in AL and GA. The sites in North Carolina (JOKM, SHRO, LIGO) and Tennessee (GRSM) show the greatest response to emission reductions in TN. The sites in Virginia and West Virginia (JEFF, SHEN, OTRC, DOSO) show the greatest response to emission reductions in WV, VA, and the Midwest sub-domain.

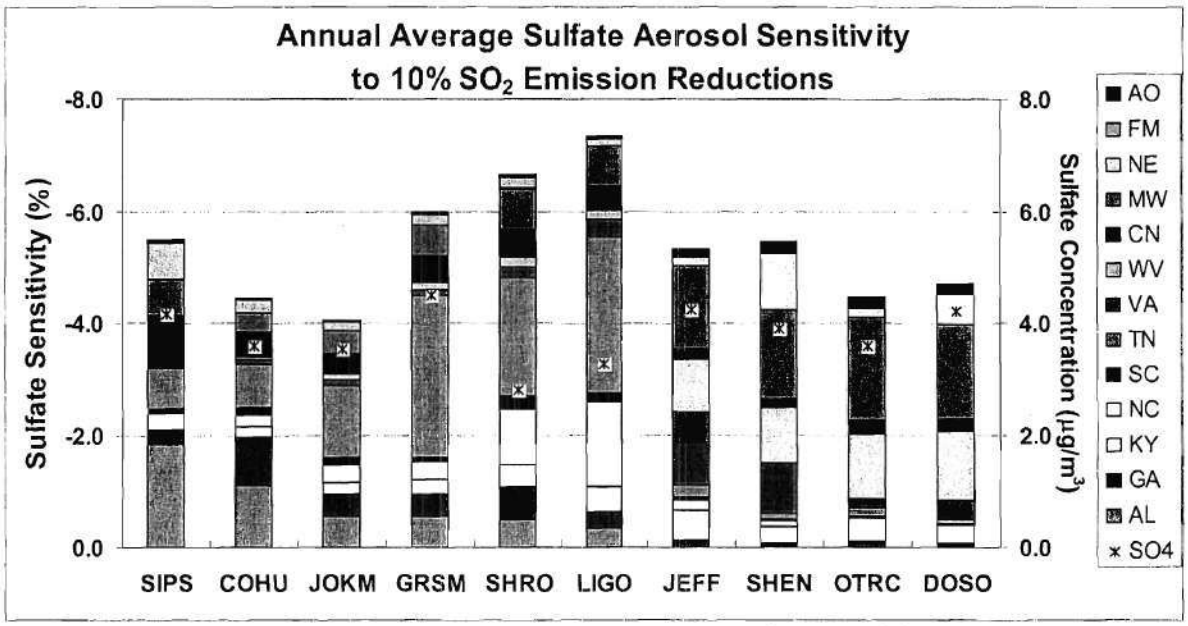

Figure 8: Annual average fine sulfate concentrations (*) and sensitivities for ten Class I areas to a 10% reduction in SO_2 emissions from each geographic sub-domain.

Figures 9-11, show the response of nitrate, ammonium, and $PM_{2.5}$ to reductions in SO_2 emissions. Nitrate increases between 1.2% and 4.2% and ammonium decreases between 1.9% and 4.2%. The increase in nitrates is due to the increase in free ammonia gas that becomes available when sulfate concentrations decrease. Ammonium does not decrease as much as sulfate because of the increase in ammonium nitrate. Approximately half of the $PM_{2.5}$ contains species that are not affected by reductions in SO_2 emissions leading to $PM_{2.5}$ reductions that are typically in the range of 1.7% to 2.7%.

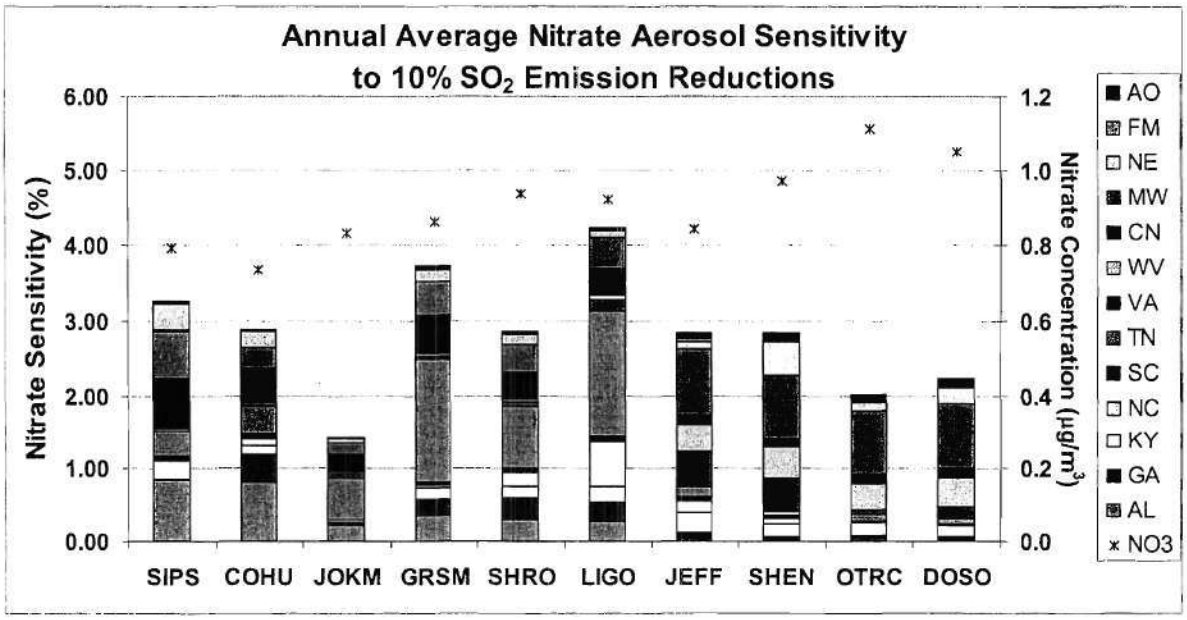

Figure 9: Annual average fine nitrate concentrations (*) and sensitivities for ten Class I areas to a 10% reduction in SO_2 emissions from each geographic sub-domain. Note, in this case nitrate increases as SO_2 is decreased.

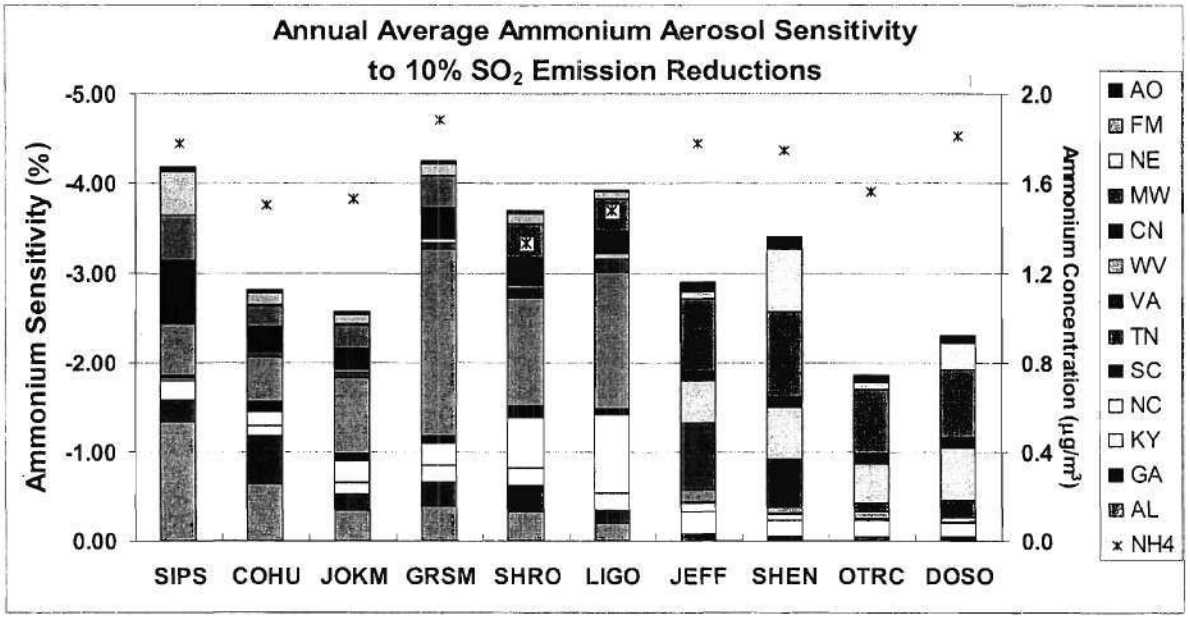

Figure 10: Annual average fine ammonium concentrations (*) and sensitivities for ten Class I areas to a 10% reduction in SO_2 emissions from each geographic sub-domain.

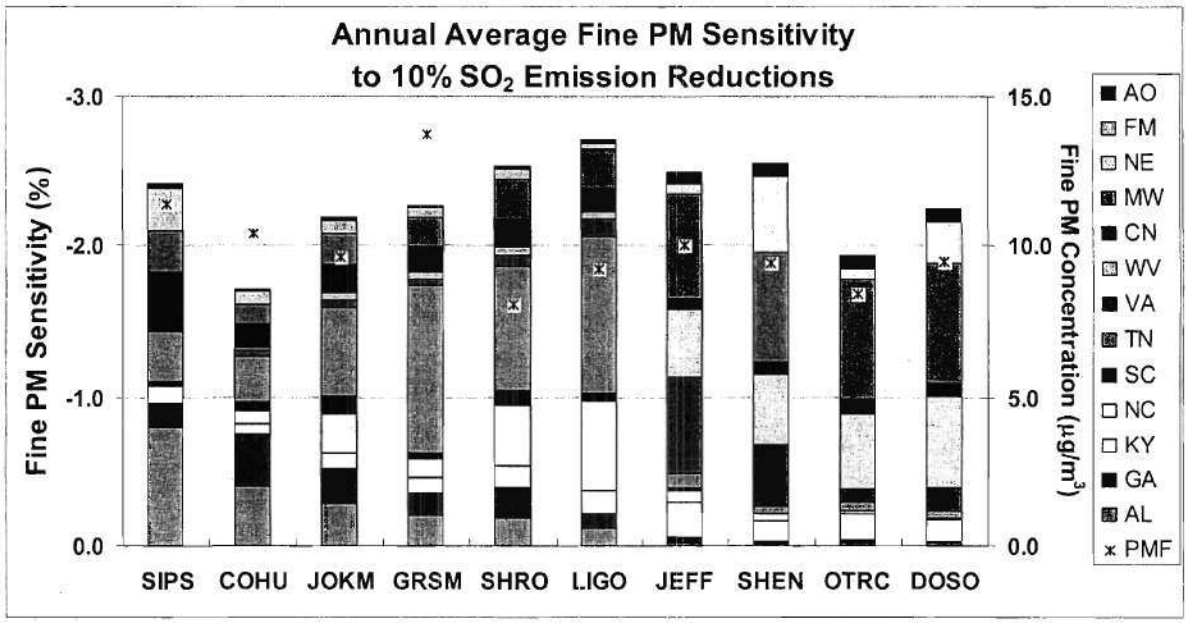

Figure 11: Annual average fine PM concentrations (*) and sensitivities for ten Class I areas to a 10% reduction in SO_2 emissions from each geographic sub-domain.

A normalized sensitivity can be calculated by dividing the percent reduction from a specific sub-domain by the total percent reduction from the entire domain, indicating the fractional contribution of the sub-domain to the domain-wide sensitivity. Figure 12 shows the normalized annual average fine PM concentrations and sensitivities for ten

Class I areas to a 10% reduction in SO_2 emissions from different sub-domains. Although not shown here, the normalized annual average fine sulfate, nitrate, and ammonium sensitivities show nearly identical regional distributions.

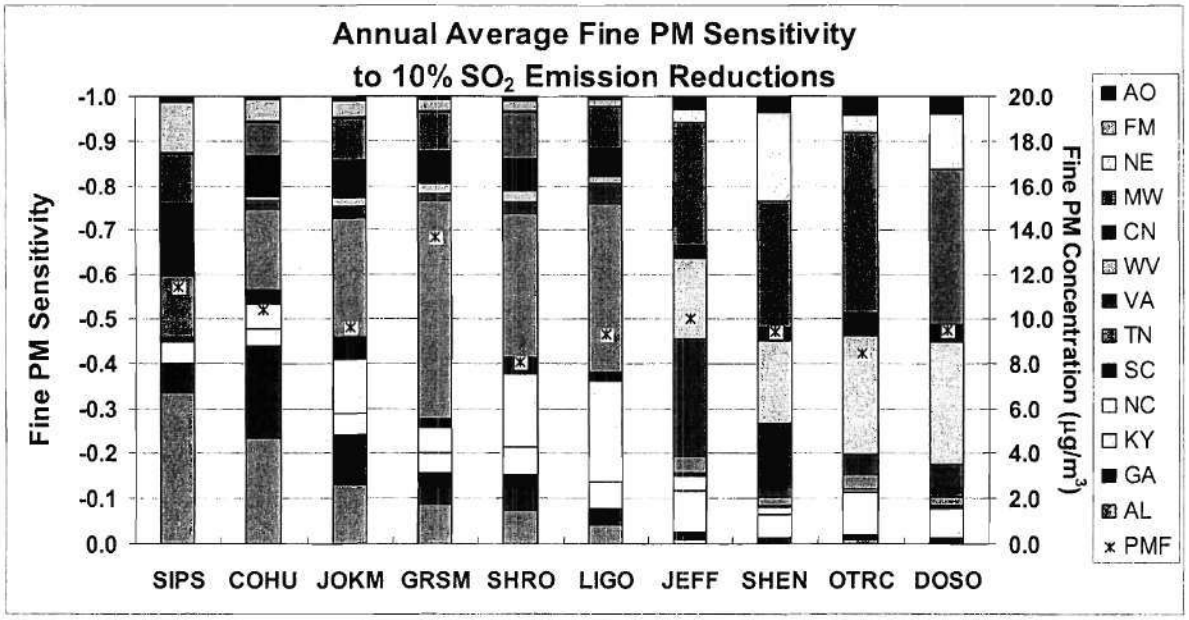

Figure 12: Annual average fine PM concentrations (•) and normalized sensitivities for ten Class I areas to a 10% reduction in SO_2 emissions from each geographic sub-domain.

Sulfate Wet Deposition Sensitivity Results

Sulfate wet deposition sensitivities to SO_2 emission reductions at eleven Class I areas (listed in Table 8) were calculated using DDM-3D. As shown in Figure 13, a 10% reduction in SO_2 emissions results in sulfate wet deposition decreasing between 4.0% and 9.2%. In general, the sulfate wet deposition sensitivities are similar to the sulfate aerosol sensitivities. However, there are some notable differences. For example, reductions in SO_2 emissions in VA show a much greater local impact on sulfate wet deposition compared to sulfate aerosol sensitivities. Consistent with the aerosol sensitivities, the sites in the Alabama and Georgia (SIPS, COHU) show high responses to emission reductions in AL and GA and the sites in Virginia and West Virginia (JEFF, SHEN, OTRC, DOSO) show high responses to emission reductions in VA, WV and the Midwest sub-domain. However, the sites in North Carolina (JOKM, SHRO, LIGO) and Tennessee (CLND, ELKM) show higher responses to emission reductions in AL and GA than did sulfate aerosols. These southern states show a greater influence on the sites in North Carolina and Tennessee because prevailing precipitation patterns carry moisture from the Gulf of Mexico across Alabama and Georgia before depositing out.

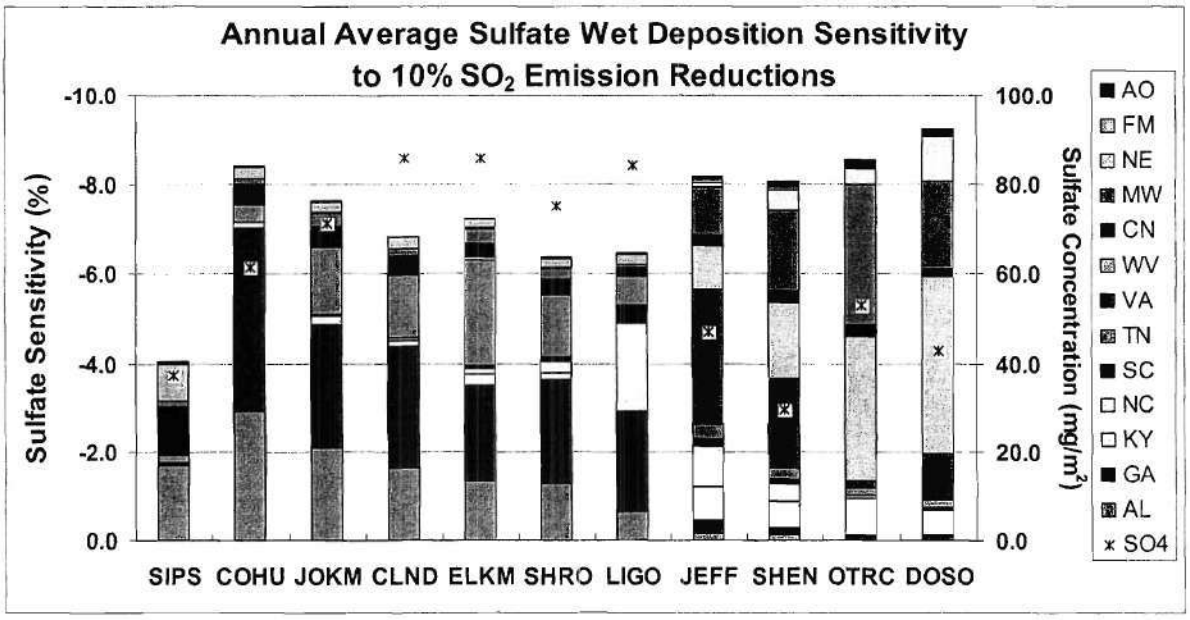

Figure 13: Annual weekly average sulfate wet deposition levels and sensitivities for ten Class I areas to a 10% reduction in SO_2 emissions from each geographic sub-domain. Note, Clingmans Dome (CLND) and Elkmont (ELKM) are both in the Great Smoky Mountains National Park.

In addition to providing regional responses to emission changes, as done here, an extension of the DDM-3D technique has been used for emission inventory assessment using an inverse modeling technique (Mendoza-Dominguez and Russell, 2001). That effort suggested that the SO_2 emission estimates for this region are relatively accurate.

REMARKS ON DIRECT SENSITIVITY ANALYSIS

The limitations of the DDM-3D method have been indicated throughout the paper. It is extremely important to understand what these limitations are before interpreting the results presented above or using the DDM-3D technique. For readers' convenience, they are restated in this section.

1. The sensitivity coefficient (or sensitivity) calculated by DDM-3D is the local slope (a point value for the level of emissions used in the simulation) of the curve that defines a pollutant concentration as a function of a single emission parameter (a certain type of emission from a given geographic region). For convenience, the sensitivity coefficients were presented above as estimated changes in pollutant concentrations due to a 10% reduction in the emission parameter. These are not actual responses to the emission reductions. In other words, no model simulation was conducted with reduced emissions but the slope was extrapolated from the simulation level to 90% of this level. If the concentration is not a linear function of the emission parameter, there is an error involved in this extrapolation.

2. A limited analysis was performed to estimate the level of emission reduction at which the extrapolation error becomes significant. Note that the analysis was performed only for the July 1995 episode and only using domain-wide reductions. Among the pollutant-emission pairs discussed above, the differences between the actual model response and the extrapolation of DDM-3D sensitivities were observed qualitatively and were deemed to be not significant up to about 30% reductions. The differences may be larger for other episodes, reductions from an individual state or region, or for reductions beyond 30%.

3. The sensitivities are calculated for reductions in a single emission parameter at a time. Here the emission parameter was the SO_2 emissions from a single sub-domain (e.g., state or region). The sensitivities were stacked in charts for convenient comparison to the emission reductions from different sub-domains. Limited analysis has shown that the error involved in superposing sensitivities from different sub-domains was not significant for the level of reductions discussed here. However, note that this error may compound the extrapolation error.

4. A more significant error may result if the sensitivities to reductions in different emission source types but from the same sub-domain were superposed. For example, the response of nitrate aerosol to simultaneous reductions of NO_x and SO_2 from the same state may be substantially different then the superposed sensitivities to individual reductions.

5. The grid used did not have the same resolution everywhere. The finest resolution was placed over the SAMI region. Some of the outer sub-domains (e.g., Central region) were covered with very coarse grid resolution. Therefore, the sensitivities to emission reductions from regional sub-domains are less reliable than those from SAMI states.

6. Finally, DDM-3D sensitivities may be used as indicators in the initial stages of control strategy design, but the effectiveness of the design should always be checked with full-scale modeling.

CONCLUSIONS

DDM-3D was extended to calculate particulate matter and wet deposition sensitivities in addition to gas-phase sensitivities. This allows many sensitivity coefficients to be calculated simultaneously. The sensitivity results obtained using the DDM-3D technique were nearly identical to those produced using the "brute force" method for most pollutants. The DDM-3D sensitivity technique was then applied to the SAMI integrated assessment for a first-order estimate of how future pollutant levels respond to emission changes. Here, the response of particulate matter and sulfate wet deposition were calculated for a 10% reduction in SO_2 emissions. SO_2 emission

reductions from different geographic regions displayed very different levels of impact on various sites within the SAMI region. In general, sites showed the greatest response to emission reductions in the nearest sub-domains. Sulfate aerosol concentrations were reduced by 4.0% - 7.3% in response to 10% reductions in SO_2 from each sub-domain. Nitrate increased between 1.2% and 4.2%, ammonium decreased between 1.9% and 4.2%, and $PM_{2.5}$ decreased by 1.7 to 2.7% in response to SO_2 reductions of 10%. Sulfate wet deposition showed reductions similar to sulfate aerosol, but the impacts of sulfate wet deposition were more localized for sites in AL, GA, WV, and VA. Similar techniques can be used to look at the response of ozone, aerosol, and wet deposition to other emissions (e.g., NO_x and NH_3). This information can be used to guide the development of control strategies, since it gives some directional sense to where to look for emission reductions. However, DDM-3D should not be substituted for full scale modeling to demonstrate the effectiveness of a given strategy.

Acknowledgements – This research was sponsored by the Southern Appalachian Mountain Initiative (SAMI) under grants from the U.S. Environmental Protection Agency to Georgia Tech and the California Institute of Technology (R826371-01). While this project was funded, in part, by the US EPA, it has not been subjected to any EPA review and does not necessarily reflect the agency's endorsements.

REFERENCES

Ansari A.S. and Pandis S.N. (1999) Prediction of multicomponent inorganic atmospheric aerosol behavior. *Atmos. Environ.* 33, 745-757.

Bergin M.S., Russell A.G. and Milford J.B. (1998) Effects of chemical mechanism uncertainties on the reactivity quantification of volatile organic compounds using a three-dimensional air quality model. *Environ. Sci. Technol.* 32, 694-703.

Berkowitz C.E., Easter R.C. and Scott B.C. (1989) Theory and results from a quasi-steady-state precipitation-scavenging model. *Atmos. Environ.* 23, 1555-1571.

Boylan J.W., Odman M.T., Wilkinson J.W., Russell A.G., Doty K.G., Norris W.B. and McNider R.T. (2002a) Development of a comprehensive, multiscale "one atmosphere" modeling system: application to the Southern Appalachian Mountains. *Atmos. Environ.*, in press.

Boylan J.W., Odman M.T., Wilkinson J.W., Russell A.G., Doty K.G., Norris W.B., McNider R.T., Mueller S.F., and Imhoff R.E. (2002b) Performance evaluation of the URM-1ATM modeling system in the Southern Appalachian Mountains. Submitted to *J. Air Waste Manage Assoc.*

Boylan J.W., Odman M.T., Wilkinson J.W., Russell A.G., Mueller S.F., Imhoff R.E., and Brewer P.F. (2002c) Response of ozone, $PM_{2.5}$, and acid deposition in the Southern Appalachian Mountains to future year emission scenarios. Submitted to *Environ. Sci. Technol.*

Carter W.P.L. (1990) A detailed mechanism for the gas-phase atmospheric reaction of organic compounds. *Atmos. Environ.* 24, 481-518.

Carter W.P.L. (1995) Computer modeling of environmental chamber measurements of maximum incremental reactivities of volatile organic compounds. *Atmos. Environ.* 29, 2513 – 2527.

Cowling E.B. (1998) Recent changes in chemical climate and related effects on forests in North America and Europe. *AMBIO* 18, 167-171.

Deuel H.P. and Douglas S.G. (1998) *Episode selection for the integrated analysis of ozone, visibility and acid deposition for the Southern Appalachian Mountains*; Systems Applications International, Inc.: San Rafael, CA. SYSAPP-98/07r1.

Dunker A.M. (1981) Calculation of sensitivity coefficients for complex atmospheric models. *Atmos. Environ.* 15, 1155-1161.

Dunker A.M. (1984) The decoupled direct method for calculating sensitivity coefficients in chemical kinetics. *J. Chem. Phys.* 81, 2385-2393.

Friedlander S.K. (1977) Smoke, Dust, and Haze. Wiley, New York (1977).

Harley R.A., Russell A.G., McRae G.J., Cass G.R. and Seinfeld J.H. (1993) Photochemical modeling of the Southern California Air Quality Study. *Environ. Sci. Technol.* 27, 378-388.

Heck W.W., Furiness C.S., Cowling E.B. and Sims C.K. (1998) Effects of ozone on crop, forest, and natural ecosystems: assessment of research needs, *EM*. October, 11-22.

Kumar N., Odman M.T. and Russell A.G. (1994) Multiscale air quality modeling: Application to Southern California. J. Geophys. Res. 99, 5385-5397.

Mendoza-Dominguez A. and Russell A.G. (2001) Estimation of emission adjustments from the application of four-dimensional data assimilation to photochemical air quality modeling. *Atmos. Environ.* 35, 2879-2894.

McNair L., Russell A. and Odman M.T. (1992) Airshed calculation of the sensitivity of pollutant formation to organic compound classes and oxygenates associated with alternative fuels. *J. Air & Waste Manage. Assoc.* 42, 174-178.

NPS (2000). National Park Service Air Quality Research Division Fort Collins. Anonymous ftp at ftp://alta_vista.cira.colostate.edu in /data/improve.

Neses A., Pilinis C. and Pandis S.N. (1998) ISORROPIA: A new thermodynamic equilibrium model for multiphase multicomponent inorganic aerosols. *Aquatic Geochemistry*. 4, 123-152.

Odman M.T. and Russell A.G. (1991a) Multiscale modeling of pollutant transport and chemistry. *J. Geophys. Res.* 96, 7363-7370.

Odman M.T. and Russell A.G. (1991b) A multiscale finite element pollutant transport scheme for urban and regional modeling. *Atmos. Environ.* 25A, 2385-2394.

Pandis S.N., Harley R.A., Cass G.R. and Seinfeld J.H. (1992) Secondary organic aerosol formation and transport. *Atmos. Environ.* 26A, 2269-2282.

Pandis S.N., Wexler S.W. and Seinfeld J.H. (1993) Secondary organic aerosol formation and transport-II. Predicting the ambient secondary organic aerosol size distribution. *Atmos. Environ.* 27A, 2403-2416.

Pechan /Avanti Group, 2001. *Southern Appalachian Mountains Initiative (SAMI) Emissions Projections to 2010 and 2040: Growth and Control Data and Emission Estimation Methodologies*. Draft Final Report # 01.07.002/9405.000.

Pielke R.A., Cotton W.R., Walko R.L., Tremback C.J., Lyons W.A., Grasso L.D., Nicholls M.E., Moran M.D., Wesley D.A., Lee T.J. and Copeland J.H. (1992) A comprehensive meteorological modeling system - RAMS. *Meteor. Atmos. Phys.* 49, 69-91.

Russell A.G., McCue K.F. and Cass G.R. (1988) Mathematical modeling of the formation of nitrogen-containing air pollutants. I. Evaluation of an Eulerian photochemical model. *Environ. Sci. Technol.* 22, 263-271.

SAMI (2001) Southern Appalachian Mountains Initiative 2001 Interim Report.

Seigneur C. (2001) Current status of air quality models for particulate matter. *J. Air & Waste Manage. Assoc.* 51, 1508-1521.

Seigneur C., Tonne C., Krishnakumar V., Pai P. and Levin L. (2000) The sensitivity of $PM_{2.5}$ source-receptor relationships to atmospheric chemistry and transport in a three-dimensional air quality modeling. *J. Air & Waste Manage. Assoc.* 50, 428-435.

Sisler J.F. and Malm W.C. (2000) Interpretation of Trends of $PM_{2.5}$ and Reconstructed Visibility from the IMPROVE Network. *J. Air & Waste Manage. Assoc.* 50, 775-789.

USEPA (1990) Section 112 of the Clean Air Act Amendments. http://www.epa.gov/ttn/atw/mactfnl.html.

USEPA (1998) 40 CFR Parts 51, 72, 75, and 96. Federal Register Vol. 63, No. 207, 57356-57538.

USEPA (1999) *Draft Guidance on the Use of Models and Other Analyses in Attainment Demonstrations for the 8-Hour Ozone NAAQS.* EPA-454/R-99-004.

USEPA (2001) 40 CFR Parts 80 and 86. Federal Register Vol. 66, No. 72, 19295-19311.

Wilkinson J.G., Loomis C.F., McNally D.E., Emigh R.A. and Tesche T.W. (1994) *Technical Formulation Document: SARMAP/LMOS Emissions Modeling System (EMS-95).* AG-90/TS26 & AG-90/TS27. Alpine Geophysics, Pittsburgh, PA.

Winner D.A., Cass G.R. and Harley R.A. (1995) Effect of alternative boundary conditions on predicted ozone control strategy performance: A case study in the Los Angeles area. *Atmos. Environ.* 29, 3451-3464.

Yang Y.J., Wilkinson J.W. and Russell A.G. (1997) Fast, direct sensitivity analysis of multidimensional photochemical models. *Environ. Sci. Technol.* 31, 2859-2868.

PERGAMON

Atmospheric Environment 36 (2002) 3721–3734

ATMOSPHERIC ENVIRONMENT

www.elsevier.com/locate/atmosenv

Development of a comprehensive, multiscale "one-atmosphere" modeling system: application to the Southern Appalachian Mountains

James W. Boylan[a,*], Mehmet T. Odman[a], James G. Wilkinson[a], Armistead G. Russell[a], Kevin G. Doty[b], William B. Norris[b], Richard T. McNider[b]

[a] *Department of Civil and Environmental Engineering, Georgia Institute of Technology, Daniel Laboratory, 200 Bobby Dodd Way, Atlanta, GA 30332-0512, USA*

[b] *University of Alabama, Huntsville, AL 35899, USA*

Received 5 September 2001; accepted 28 May 2002

Abstract

A comprehensive three-dimensional Eulerian photochemical model (URM-1ATM) was developed that simulates urban and regional gas and size-resolved aerosol concentrations of pollutants in the atmosphere and both wet and dry deposition. In this study, RAMS and EMS-95 are used to generate meteorological and emission input files, respectively. The modeling system is then applied to simulate the evolution, transport, and removal of atmospheric pollutants over the Eastern US for the 11–19 July 1995 episode. Performance statistics are calculated for ozone, speciated fine particles, and acid deposition mass fluxes.

Keywords: Mathematical modeling; Ozone; Aerosols; Wet deposition

1. Introduction

Photochemical air quality models are used extensively in both scientific studies and regulatory applications. They integrate our understanding of the complex chemical and physical processes that govern the formation, transport and removal of gas- and aerosol-phase pollutants in the atmosphere. These mathematical models use emission inputs, meteorological inputs, and a description of the atmospheric chemistry to predict pollutant concentrations. They are critical in developing optimal emissions control strategies to reduce atmospheric pollutants in urban and rural areas. In the past, air quality model applications focused either on acid deposition or ozone impacts individually and not collectively under a "one-atmosphere" approach. The concept of "one-atmosphere" modeling did not seem practical until recently (Russell and Dennis, 2000). This is, in part, due to the large computational resources required for particulate matter (PM) modeling (Zhang et al., 1999). Now that computational power is more readily available, "one-atmosphere" models are beginning to emerge (Byun and Ching, 1999). Although not presented in this paper, analysis has shown that there can be significant impacts on ozone concentrations in certain regions when aerosol and wet scavenging processes are included in the calculations. Also, there can be significant impacts on PM concentrations when cloud processes are considered.

The urban-to-regional multiscale (URM) model and its monoscale predecessor, the California/Carnegie Institute of Technology (CIT) model, have been widely used for simulating photochemical air pollutant dynamics. The URM model (Kumar et al., 1994; Kumar and Russell, 1996; Odman and Russell, 1991a) is a three-dimensional Eulerian photochemical model that uses a

*Corresponding author.

E-mail address: jboylan@themis.ce.gatech.edu (J.W. Boylan).

1352-2310/02/$ - see front matter
PII: S1352-2310(02)00356-4

finite element, variable mesh transport scheme (Odman and Russell, 1991b) along with the SAPRC chemical mechanism (Carter, 1990, 1995) for simulating the gas-phase reaction kinetics. URM uses variable size grids in its horizontal domain to effectively capture the details of pollution dynamics without being computationally intensive. By using fine grids over the source and/or receptor areas, more satisfactory predictions of both urban and regional pollutant levels can be obtained (Kumar et al., 1994).

URM has been enhanced to include aerosol dynamics through an equilibrium based aerosol module (Nenes et al., 1998; Ansari and Pandis, 1999), wet deposition scavenging processes through the reactive scavenging module (Berkowitz et al., 1989), and heterogeneous sulfate chemistry. The enhanced version of URM, called URM-1ATM, is an integrated "one-atmosphere" air quality model. As an integrated multipollutant model, the results from URM-1ATM can be used as inputs to access the effects of ozone, aerosols, and wet deposition on forests, streams, visibility, and human health.

2. Model description

The URM-1ATM model accounts for transport and chemistry of pollutants by solving the atmospheric diffusion equation.

$$\frac{\partial c_i}{\partial t} + \nabla \cdot (\mathbf{u}c_i) = \nabla \cdot (\mathbf{K}\nabla c_i) + f_i + S_i. \quad (1)$$

Here, c_i is the concentration of the ith pollutant among p species, i.e., $i = 1, \ldots, p$, $\mathbf{u}$ describes the velocity field, $\mathbf{K}$ is the diffusivity tensor, $f_i(c_1, \ldots, c_p)$ is the chemical reaction term and S_i is the net source term. Elevated emissions and removal processes other than wet and dry deposition are included in S_i. The equations and assumptions describing the horizontal and vertical boundary conditions can be found in Kumar and Russell (1996).

In solving the atmospheric diffusion equation, URM-1ATM uses operator splitting and decouples various processes. The operator splitting approach advances the solution in time as

$$c^{n+1} = L_{xy} L_{\text{Emis}} L_{\text{Hetero}} L_{\text{Advec}} L_{\text{Chem}} L_{\text{Aero}} L_{\text{Wet}} L_{xy} c^n, \quad (2)$$

where L_{xy} is the horizontal advection and diffusion transport operator, L_{Emis} the elevated point source emissions operator, L_{Hetero} the S(IV) to S(VI) aqueous-phase heterogeneous chemistry operator, L_{Advec} the vertical advection operator, L_{Chem} the coupled vertical diffusion, gas-phase chemistry, area source emissions, and dry deposition operator, L_{Aero} the aerosol condensation/evaporation and growth operator, and L_{Wet} the wet deposition and scavenging operator.

The time step for each process is determined dynamically based on stability and accuracy considerations. A more detailed treatment of each of these processes will be discussed in the following sections.

2.1. Transport processes

URM-1ATM uses the two-dimensional streamline upwind Petrov–Galerkin (SUPG) finite element method for solving the horizontal advection equations (Odman and Russell, 1991a, b). The SUPG is a high-order accurate scheme, but is not monotonic or positive definite. To avoid negative concentrations, the SUPG finite element solution is followed by application of a mass conservative isotropic diffusion filter (Odman and Russell, 1993). URM-1ATM treats vertical advection through the use of first-order upwind differencing. To avoid mass conservation problems, the vertical velocities are adjusted by solving the continuity equation using the same numerical techniques (Odman and Russell, 2000). This adjustment has little effect on vertical transport.

To account for convective cloud processes and pollutant scavenging (discussed later), the reactive scavenging module (Berkowitz et al., 1989; Scott, 1987) has been incorporated into URM-1ATM. Convective precipitation is simulated with a two-cell (stratiform and convective), steady-state model. This approach allows the definition of several characteristics of convective clouds including large updrafts and vertical transport of low-level air to upper levels. Table 1 contains the transported gas-phase species, transported aerosol species, and the steady-state species incorporated in URM-1ATM. Constant species include oxygen, methane, carbon dioxide, and hydrogen.

2.2. Chemistry processes

The gas-phase reaction kinetics are simulated using the SAPRC chemical mechanism (Carter, 1990), which has been updated with a more accurate treatment of isoprene (Carter, 1995). This mechanism accounts for the atmospheric oxidation of over 100 reactive organic compounds (e.g., alkanes, alkenes, aromatics, alcohols, ethers) as well as a number of reactive oxygenated and organic nitrate products.

Aqueous-phase chemistry is based on the reactions implemented in the RSM. It includes the heterogeneous reactions of S(IV) with peroxides and ozone (when the droplet is neutral or basic) to form S(VI). Hydrogen ion concentrations in cloud water and rain are calculated from an electroneutrality equation, based on the concentrations of anions such as sulfate and nitrate, and cations such as ammonium and other positive ions associated with crustal material. Gas-phase reactions produce secondary organic aerosols by using lumped

Table 1
Species used in the URM-1ATM model

Transported gas-phase species	Transported gas-phase species	Transported gas-phase species	Transported aerosol species	Steady-state species
NO[a]—nitric oxide	RRP—RO_2-RO_2-product	M2BT—2-methyl-2-butene	SODX[a,b]—sodium	OSD—O*1D2, O singlet D
NO_2[a]—nitrogen dioxide	RHP—RO_2-HO_2-product	AAR1[a]—general alkane and aromatics	HYDX[b]—hydrogen	O—oxygen atom
O_3—ozone	OLRI—OLD-RI, O atom reactions with olefins	AAR2[a]—general alkane and aromatics	AMNX[b]—ammonium	HO—hydroxyl radical
HONO—nitrous acid	O_3SB—O_3OL-SB, represents conversion of SO_2 to SO_3	AAR3[a]—general alkane and aromatics	NITX[a,b]—nitrate	CCO—CCO-O_2 radical
HNO_3—nitric acid	MEOH[a]—methanol	OLE1[a]—general alkenes	CHLX[b]—chloride	C_2CO—C_2CO-O_2 radical
HNO_4—peroxynitric acid	ETOH[a]—ethanol	OLE2[a]—general alkenes	SULX[a,b]—sulfate	BCO_2—BZ-CO-O_2 radical
N_2O_5—nitrogen pentoxide	GLY—gluoxal	NH_3[a]—ammonia	WATX[b]—water	RO_2N—alkyl nitrate RO_2 radical
NO_3—nitrate radical	RNO_3—organic nitrates	SO_2[a]—sulfur dioxide	CARX[a,b]—elemental carbon	RO_2X—RO_2-XN radical
HO_2—hydroperoxy radical	GPAN—glyoxyl developed PAN	SO_3—sulfur trioxide, rapidly forms H_2SO_4	ORGX[a,b]—organics	RO_2P—RO_2-NP, phenol RO_2 radical
CO[a]—carbon monoxide	PHEN—phenol	APNE[a]—α-pinene	CRMX[a,b]—magnesium	RO_2R—general RO_2 No. 1 radical
HCHO[a]—formaldehyde	TOLU[a]—toluene	UNKN—unknown	CRKX[a,b]—potassium	R_2O_2—general RO_2 No. 2 radical
MEK[a]—methylethyl ketone	BALD—benzaldehyde	PRPA—propane	CRCX[a,b]—calcium	COCO—HCOCO-O_2 radical
MGLY—methyl glyoxyl	PBZN—peroxy benzoyl nitrate	MARC—methracloin	PMX[a,b]—other PM	HCO_3—HOCOO radical
PAN—peroxyacetyl nitrate	AFG1—aromatic ring fragments 1	MVK—methyl vinyl ketone		BZO—phenoxy radical
MPAN—methyl peroxyacetyl nitrate	AFG2—aromatic ring fragments 2	IPRD—isoprene reaction prods.		BZNO—$BZ(NO_2)$-O
RO_2—alkyl peroxy radicals	CCHO[a]—acetaldehyde	MRC3—methyl peroxyacetyl radical		
RCO_3—peroxyacyl radical	RCHO—propionaldehyde and all higher aldehydes	AIR—air		
ETHE[a]—ethene	ACET[a]—acetone	INRT—inert		
CRES—cresols and other alkyl phenols	PPN—peroxy propionyl nitrate	HCl—hydrochloric acid		
NPHE—nitrophenols	PRPE—propene	ORGG—gas-phase condensable organics		
HO_2H—hydrogen peroxide	M1BT—2-methyl-1-butene			
C—carbon atoms	ISOP[a]—isoprene			
LN—lost nitrogen atoms				
OOH—lumped hydroperoxy species				

[a] Emission species generated by EMS-95.

[b] X represents the different aerosol size bins: $X = 1$ represents aerosols $<0.156\,\mu m$, $X = 2$ represents aerosols from 0.156 to $0.625\,\mu m$, $X = 3$ represents aerosols from 0.625 to $2.5\,\mu m$, and $X = 4$ represents aerosols from 2.5 to $10.0\,\mu m$.

experimental and estimated organic aerosol yields (Pandis et al., 1992).

2.3. Aerosol module

The aerosol module is capable of simulating concentrations of all major primary and secondary components of atmospheric PM. There are three groups of aerosol species that are considered in the aerosol routine: inert species, inorganic equilibrium species, and organic species. The inert species include magnesium, potassium, calcium, elemental carbon, and a group that includes all other inert PM species. The inorganic equilibrium species include sulfate, nitrate, ammonium, sodium, chloride, and hydrogen ion. The organic aerosols are represented by a lumped species that contains numerous condensable organics resulting from the oxidation of organic gases and directly emitted organic particles.

The aerosol particles are assumed to be internally mixed, meaning that all particles of the same size have the same composition. A sectional approach is used for characterization of the continuous aerosol size distribution by using four size bins: particle diameters <0.156, 0.156–0.625, 0.625–2.5, and 2.5–10.0 μm. The module simulates mass transfer and particle growth occurring between the gaseous and aerosol species (Pandis et al., 1993). ISORROPIA (Nenes et al., 1998) is used to simulate the condensation and evaporation of inorganic atmospheric aerosols. ISORROPIA is a computationally efficient and rigorous thermodynamic model that predicts the physical state and composition of the sodium–ammonium–chloride–sulfate–nitrate–water aerosol system. The possible species for each phase include:

Gas : NH_3, HNO_3, HCl, H_2O,

Liquid : $NH_4^+, Na^+, H^+, Cl^-, NO_3^-, SO_4^{2-}$, HSO_4^-, OH^-, H_2O,

Solid : $(NH_4)_2SO_4, NH_4HSO_4, (NH_4)_3H(SO_4)_2$, $NH_4NO_3, NH_4Cl, NaCl, NaNO_3, NaHSO_4$, Na_2SO_4, and H_2SO_4.

The 15 equilibrium reactions that are computed in the ISORROPIA mechanism in conjunction with their equilibrium constants can be found in Nenes et al. (1998). The aerosol mass that is condensed or evaporated in the ISORROPIA routine is partitioned among each size bin based on the original size distribution. Then, the movement of these sections in the size coordinate as a result of particle growth is calculated using the moving section technique (Gelbard, 1990; Kim and Seinfeld, 1990).

The production of condensable organic species from the oxidation of gaseous organic compounds is based on experimental and estimated organic aerosol yields (Pandis et al., 1992). The formation of condensable organic aerosol species is performed in the chemistry module and is assumed to be irreversible. The distribution and growth of condensed organic aerosols to the four size bins is simulated in the aerosol routine. Also, an algorithm to simulate particle deposition and gravitational settling for particles of various sizes has been added. Inputs to the aerosol module include temperature, relative humidity, air density, and gas and aerosol concentrations. Outputs from the module are the updated equilibrium concentrations for the gas-phase and aerosol species.

2.4. Wet deposition and scavenging processes

The reactive scavenging module (Berkowitz et al., 1989) uses synoptic scale temperature and precipitation rates to simulate a field of representative clouds that are defined by scavenging rates, water profiles, and wind fields. The module simulates the time dependent chemical kinetic interaction of these clouds with the gas and aerosol species and the vertical convective transport within a column of air. RSM simulates the aqueous-phase oxidation of S(IV) to S(VI) by hydrogen peroxide and ozone. The mechanism does not consider catalytic conversion by iron and other metals due to the uncertainty in the reaction pathways and uncertainties in the emissions of metals. The module also considers odd nitrogen aqueous-phase chemistry. Aqueous-phase chemistry for non-precipitating clouds are treated outside the RSM module and utilizes a simplified oxidation pathway for S(IV) by hydrogen peroxide and ozone. Scavenging processes within the module include gas, aerosol, and microphysical scavenging. Scavenging of gas-phase species by cloud water is modeled via an equilibrium process that is based on species solubilities, while scavenging by rain water is modeled for most species via mass transfer. Scavenging by snow is limited to nitric acid. Aerosol scavenging is treated by nucleation and by inertial impaction processes. The scavenged species are sulfur dioxide, aerosol sulfate, ozone, nitric acid, aerosol nitrate, hydrogen peroxide, ammonia, ammonium aerosol, and soluble crustals (Mg^{2+} and Ca^{2+}). Other gas and aerosol species are passed into the RSM module where vertical convective transport is simulated. Output from the module includes updated concentration profiles for all the species affected by scavenging and convective cloud transport, in addition to wet deposition mass fluxes for SO_2, SO_4^{2-}, NO_3^-, H_2O_2, NH_4^+, Mg^{2+}, Ca^{2+}, and H-ion.

2.5. Dry deposition processes

For dry deposition, URM-1ATM uses the three-resistance approach based on the formulation of Wesely

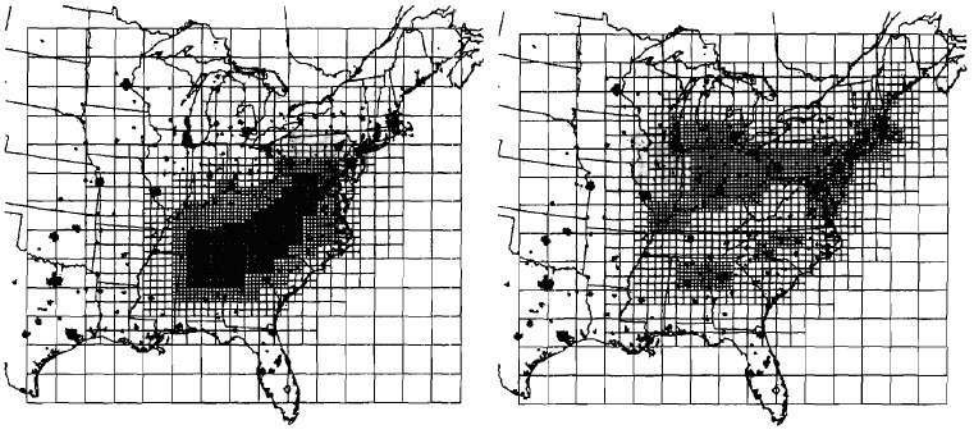

Fig. 1. Example of multiscale grid designs used in the URM-1ATM model. Grid 1 (left) places an emphasis on pollution receptor areas, while Grid 2 (right) places an emphasis on emission source areas.

(1989). Total resistance (r_t^i) to deposition of species i is composed of three resistances:

$$r_t^i = r_a + r_b + r_s^i, \tag{3}$$

where r_a is the resistance to deposition due to turbulent transport through the atmosphere, r_b is the resistance due to diffusion through a laminar sub-layer, and r_s is the resistance due to chemical interaction between the surface and the pollutant of interest. The deposition velocity (v_g^i) for species i then becomes:

$$v_g^i = \frac{1}{r_t^i}. \tag{4}$$

A detailed description of the calculation of the various resistances is given in Russell et al. (1990) and Harley et al. (1992).

For the aerosol particles, size-dependent deposition resistances are calculated using experimental data from the National Center for Atmospheric Research (1982). The aerosol deposition resistances are estimated using the log-mean diameter for each size bin and are independent of the species composition.

3. URM-1ATM modeling grids

URM differs from other air quality models in the way it provides a multiscale modeling capability. While other models resort to grid nesting techniques, URM provides a single grid with variable resolution. The finest grids are placed over the target area of interest and the adjacent areas that are expected to most directly influence the air quality in that region. Coarser cells are placed in areas that are not expected to significantly contribute to the air quality in the region of interest with the coarsest cells typically near the boundary of the domain.

In this paper, the URM-1ATM modeling domain covers the eastern half of the United States. Two example modeling grids are shown in Fig. 1. The first grid emphasizes a pollution receptor area and has the finest grid resolution (12 km) over the Appalachian Mountains. The second grid places an emphasis on emission source areas and has the finest grid (24 km) over areas of high emissions (e.g., urban areas and the Ohio River Valley). The grid dimensions double from the smaller grid to the next larger grid size, with the largest grid at 192 km. Grid 1 is used for the performance evaluation presented later in this paper. The modeling domain extends from the surface to a height of 12,867 m, consistent with the vertical extent of the meteorological modeling domain, and is divided into seven vertical layers with thickness of 19, 43, 432, 999, 1779, 3588, and 6007 m, respectively. The use of finer resolution near the surface of the domain, as compared to the coarser resolution aloft, allows the steeper concentration gradients that typically exist in the boundary layer and the evolution of the mixing depths during the day to be captured with greater detail.

4. URM-1ATM model inputs

URM-1ATM requires estimates of the meteorology, emissions, and air quality fields. For purposes of this study, meteorological predictions are taken from the regional atmospheric modeling system (RAMS) (Pielke et al., 1992), and emissions estimates are prepared using the emissions modeling system (EMS-95) (Wilkinson

et al., 1994). The observed air quality fields are used for setting the initial and boundary conditions. Other inputs include landuse, dry deposition resistances, and surface roughness.

4.1. Meteorological modeling

A modified version of the RAMS (Pielke et al., 1992) version 3a has been used to produce meteorological input fields for URM-1ATM. It was run with a system of three nested grids in non-hydrostatic mode with cloud and rain water microphysics activated. The National Center for Environmental Prediction (NCEP)/National Center for Atmospheric Research (NCAR) reanalysis data (Kalnay et al., 1996) was chosen as the main data source for the meteorological simulations. The nested grid structure consisted of 48-, 24-, and 12-km resolution grids for some applications, while 96-, 24-, and 12-km resolution grids were used for others. The modeling results that will be analyzed later in this paper used the 48-, 24-, and 12-km resolution grids. Before these fields can be used, they must be converted from the RAMS nested grid structure to the URM-1ATM multiscale grid structure. The grid nests in RAMS are arranged such that there is always meteorological data available at the resolution of the URM-1ATM grid. For example, the 12-km RAMS grid is a rectangle that covers the entire 12-km resolution portion of Grid 1 in Fig. 1. Within the rectangle, the URM-1ATM grids use 12 km grid cells as well as coarser grid cells (e.g. 24 or 48 km). In other words, there is always a one-to-one mapping from the URM-1ATM grid to the RAMS grid (but not vice versa). Therefore, when meteorological data is converted there is no need for interpolation in the horizontal space. The conversion is actually a "restriction" or aggregation, whenever appropriate, of better resolved RAMS data. However, the RAMS and URM-1ATM vertical grids are slightly different. Though the two grids do match in the vertical extent (i.e. 12,867 m), the RAMS vertical structure has 31 layers, while the URM-1ATM vertical structure has seven layers. Hence, it is necessary to aggregate the higher resolution RAMS layers into the more coarse URM-1ATM layers. A simple distance-weighting scheme is used to interpolate the scalar fields in the vertical. The horizontal wind field is converted to its momentum equivalent using the predicted density field prior to interpolation of the winds in the vertical. Once the momentum field and the density field are interpolated from the RAMS vertical grid to the URM-1ATM vertical grid, the horizontal wind field is reconstructed. The parameters that are used by URM-1ATM include: ambient temperature (K); u, v, and w components of wind ($m\,s^{-1}$); air density ($kg\,m^{-3}$); mixing depths (m); absolute humidity—mixing ratio ($g\,kg^{-1}$); turbulent momentum diffusivity ($m^2\,s^{-1}$); total incoming solar radiation ($W\,m^{-2}$); total incoming ultraviolet radiation ($W\,m^{-2}$); precipitation (mm), convective cloud cover area fraction (%); convective cloud precipitation fraction (%); convective cloud top height (m); and stratiform cloud top height (m).

4.2. Emissions modeling

The EMS-95 (Wilkinson et al., 1994) is used to generate speciated day-specific, hour-by-hour gridded emission inputs to be used by URM-1ATM. EMS-95 separates the emissions into two categories: elevated point and ground-level source emissions. Ground-level sources include low-level point sources, mobile sources, anthropogenic area sources, non-road mobile sources, and biogenic sources. Point source and area source emissions estimates used in EMS-95 were based on data developed by the Pechan/Avanti Group (2001), as were on-road mobile source data (e.g. vehicle miles traveled by state, county, and roadway type; vehicle mix by state, county, and roadway type; speeds by vehicle type and roadway type) and were used to estimate on-road mobile source emissions using the EMS-95 motor vehicle emissions model (MoVEM). MoVEM uses MOBILE5b (USEPA, 1994) to compute vehicle-dependent emissions factors of CO, NO_x, and total organic gases (TOG). Biogenic emissions were estimated using US EPAs biogenic emissions inventory system, version 2 (BEIS2—Pierce and Geron, 1996; Pierce, 1996; Pierce et al., 1990). The point source emissions estimates were enriched with day specific emissions data obtained from major utility companies in the modeling region. Meteorological model results were used to estimate the temperature and radiation dependent biogenic emissions and the temperature dependent on-road mobile source emissions. Primary emissions species that are generated by EMS-95 for use in the SAPRC-based chemical mechanism utilized by URM-1ATM are identified in Table 1.

4.3. Initial and boundary conditions

URM-1ATM requires initial (IC) and boundary conditions (BC) for both gaseous and aerosol species. Initial conditions can have a major impact on the modeled concentrations at the beginning of the simulation, but the impact usually diminishes as the simulation proceeds. Many of the gaseous species of interest have relatively short lifetimes and quickly undergo chemical transformation and deposition. The impact of gas-phase ICs diminishes more quickly when compared to aerosol species. A two-day ramp-up period is used before each episode that is modeled and is generally sufficient to dampen the effect of initial conditions on gaseous species concentrations. However, fine aerosols have very low deposition velocities and longer lifetimes and can persist for longer periods. Therefore, the concentrations

of aerosol species have a stronger dependence on initial conditions and extra care must be used in setting those conditions.

The same principles apply to the boundary conditions. The lifetimes of gaseous species are usually not long enough for transport from the domain boundaries into the region of interest. However, the aerosol species can be transported considerable distances (e.g., thousands of kilometers) and they can impact the concentration of aerosols in the region of interest. The IC/BCs for the gaseous species were derived using data from the aerometric information retrieval system (AIRS) (USEPA, 2001) and the North American Research Study on tropospheric ozone for the Northeast (NARSTO-NE) (Mueller, 1998) data archives as well as data from specialized studies and smaller networks.

The gaseous species for which IC/BCs are developed include CO, SO_2, NO_x, VOCs and ozone. Initial conditions are based on observations that correspond to the time and date that the model simulation begins. Boundary conditions are based on observations that vary spatially and temporally over the duration of the modeling episode. Because the monitoring network does not correspond to the modeling grid, it is necessary to interpolate the observed values to the computational nodes on the modeling grid. For all the VOC species and CO, Dirichlet tessellation (Preparata and Shamos, 1985; Green and Sibson, 1978) is used to determine concentrations at each node on the modeling grid.

The IC/BCs for SO_2 and NO_x are treated differently since the AIRS SO_2 and NO_x monitors are often located in areas with high concentrations (e.g. downwind from power plant plumes) and interpolation using Dirichlet tessellation overestimates the initial and boundary conditions over rural areas. Therefore, the following interpolation scheme (Eqs. (5) and (6)) is used to derive SO_2 and NO_x IC/BCs such that the suspected high bias is minimized:

$$c_j = \exp\left[\frac{\sum_{i=1}^{n} \ln(c_i)/d_{ij}^2 c_i}{\sum_{i=1}^{n} 1/d_{ij}^2 c_i}\right] \quad \text{for } j = 1, g, \tag{5}$$

$$d_{ij}^2 = (x_j - x_i)^2 + (y_j - y_i)^2, \tag{6}$$

where c is the concentration, i is the observation index, n is the number of observations, j is the node index, g is the number of nodes, x is the east–west coordinate of the observation or node location, and y is the north–south coordinate of the observation or node location. This method was tested and found to produce similar levels of SO_2 and NO_x in both the urban and rural areas as compared to levels that were produced by running the model for multiple days.

The interpolation scheme that is used for ozone is an inverse distance squared weighting of the observations (Eq. (7)):

$$c_j = \left[\frac{\sum_{i=1}^{n} c_i/d_{ij}^2}{\sum_{i=1}^{n} 1/d_{ij}^2}\right] \quad \text{for } j = 1, g. \tag{7}$$

Like the SO_2 interpolation scheme, it too minimizes and localizes the impact of locally high ozone observations but not to the extent that the SO_2 interpolation does. That is, locally high ozone concentrations are more likely to influence IC/BCs at points further away from the measurements.

The IC/BC values at the top of the domain are set to free troposphere values (Seinfeld and Pandis, 1998). Linear interpolation from the ground-level values to the top of the domain is used to derive the IC/BC concentrations for layers in between. The IC/BCs for the other gas-phase species in the SAPRC chemical mechanism are set equal to zero and are allowed to evolve during the simulation.

The IC/BCs for the aerosol species were derived from the interagency monitoring of protected visual environments (IMPROVE) measurements. IMPROVE particulate matter measurements (NPS, 2000) are taken twice a week (Wednesday and Saturday) and are reported as a 24-hour average concentration for each species. Initial conditions are determined by examining the fine aerosol concentrations ($PM_{2.5}$) for the day that most closely matches with the start of each episode. In the event that the episode starts on a day that is equally close to two IMPROVE measurement days, an average of the two closest days is used. The initial conditions for each aerosol species are set to a uniform concentration across the domain. The concentration is equal to the average of all valid IMPROVE observations in the modeling domain. Interpolation is not performed due to the limited amount of data. To determine the boundary conditions for the north, west, and southwest boundaries, IMPROVE data for stations west of the modeling domain are used. Table 2 contains the URM-1ATM model species and the corresponding IMPROVE species along with any required conversion factors. Next, the IC/BC concentrations are distributed to each of the four aerosol bins according to size distributions estimated from plots given in Seinfeld and Pandis (1998). Finally, a charge balance is performed to ensure that the electoneutrality equation (ENE) is satisfied.

5. Model performance

In order to assess the URM-1ATM model represents the formation, transport, and deposition of atmospheric pollutants, the model was tested using the 11–19 July 1995 episode (9 and 10 July were used as ramp-up days). For much of the United States east of the Mississippi River and north of the Gulf coast, the weather was

Table 2
Aerosol species modeled by URM-1ATM and IMPROVE observations

Species	URM model species	IMPROVE observations
Fine sulfate	SUL1 + SUL2 + SUL3	BSO_4
Fine nitrate	NIT1 + NIT2 + NIT3	NO_3
Fine ammonium	AMN1 + AMN2 + AMN3	$(BSO_4 * 0.375) + (NO_3 * 0.29)$
Fine sodium	SOD1 + SOD2 + SOD3	NA
Fine chloride	CHL1 + CHL2 + CHL3	Cl
Fine hydrogen ion	HYD1 + HYD2 + HYD3	H
Fine elemental carbon	CAR1 + CAR2 + CAR3	EC1 + EC2 + EC3-OP
Fine organic carbon	ORG1 + ORG2 + ORG3	$(O_1 + O_2 + O_3 + O_4 + OP) * 1.4$
Fine calcium	CRC1 + CRC2 + CRC3	CA
Fine magnesium	CRM1 + CRM2 + CRM3	MG
Fine potassium	CRK1 + CRK2 + CRK3	K
Fine PM "other"	PM1 + PM2 + PM3	Not applicable
$PM_{2.5}$	SUL1 + SUL2 + SUL3 + NIT1 + NIT2 + NIT3 + ORG1 + ORG2 + ORG3 + CRK1 + CRK2 + CRK3 + CRC1 + CRC2 + CRC3 + CRM1 + CRM2 + CRM3 + PM1 + PM2 + PM3 + SOD1 + SOD2 + SOD3 + CAR1 + CAR2 + CAR3 + CHL1 + CHL2 + CHL3 + AMN1 + AMN2 + AMN3 + HYD1 + HYD2 + HYD3	MF
PM_{10}	SUL1 + SUL2 + SUL3 + SUL4 + NIT1 + NIT2 + NIT3 + NIT4 + ORG1 + ORG2 + ORG3 + ORG4 + CRK1 + CRK2 + CRK3 + CRK4 + CRC1 + CRC2 + CRC3 + CRC4 + CRM1 + CRM2 + CRM3 + CRM4 + PM1 + PM2 + PM3 + PM4 + SOD1 + SOD2 + SOD3 + SOD4 + CAR1 + CAR2 + CAR3 + CAR4 + CHL1 + CHL2 + CHL3 + CHL4 + AMN1 + AMN2 + AMN3 + AMN4 + HYD1 + HYD2 + HYD3 + HYD4	MT

dominated by high pressure at the surface and aloft with light winds, little precipitation, and daily maximum temperatures of 30°C and above. After 17–18 July, a frontal passage for much of the same area brought lower temperatures and humidity. Additional details on the meteorological conditions during this episode and the related meteorological performance statistics can be found in Doty et al. (2001). The targeted area of interest was the Class I areas in the Southern Appalachian Mountains; therefore, Grid 1 (shown in Fig. 1) was used. A performance evaluation was accomplished by comparing ozone concentrations, aerosol concentrations, and wet deposition mass fluxes to observation. The monitoring networks used for comparison include: aerometric information retrieval system (AIRS) for ozone, IMPROVE or aerosols, and national atmospheric deposition program (NADP) for wet deposition. In addition, simulated results of NO and NO_2 were compared to observations, but not presented here.

5.1. Ozone performance

There are several hundred AIRS stations within the modeling domain reporting data during the 11–19 July 1995 episode. However, some of these stations fall into coarse resolution cells where the model predictions are subject to significant smoothing and the observations are representative of much smaller scales. Therefore, only the 74 stations falling within the 12-km grid are used in the performance analysis.

In order to understand how the model performed at each site and how this performance varied throughout each day, hourly ozone plots, also known as time series plots, are used. These plots present both the hourly

estimates and observations throughout the simulation period. With the time series plot, one can determine the model's ability to reproduce the peak, the presence or absence of significant bias and errors within the diurnal cycle, and whether the "timing" of the estimated peak agrees with the observation. The two examples given here (Figs. 2 and 3) show the hourly ozone estimates and measurements in Nashville, TN (typical urban site) and the Great Smoky Mountains (GRSM) National Park, TN (typical high-elevation rural site). These sites were chosen since there were intensive experimental programs at Nashville (southern oxidant study—SOS) and GRSM (southeastern aerosol and visibility study—SEAVS) during this episode. The model underestimates the peaks for most days at GRSM and underestimates the peaks on 11, 12, and 16 July in Nashville. However, the diurnal variations and the timing of the peaks conform well with observations. The model typically misses the nighttime lows at the urban sites. This is probably due to a lack of vertical resolution. The under predictions of ozone at the high-elevation sites could be due to a lack of horizontal resolution. The modeled altitude of the site can be much lower than the actual altitude. Higher ozone values can be seen in layers 3 and 4.

The time series plots above are useful for looking at specific stations, but to get an idea of how well the model is performing over all stations, the normalized bias and error are calculated using the 74 stations falling into 12 km grid cells. In each case a normalized mean bias (NMB) and normalized mean error (NME) were calculated using Eqs. (8) and (9):

$$\mathrm{NMB} = \frac{1}{N}\sum_{i=1}^{N}\frac{(c_i^e - c_i^o)}{c_i^o} \times 100\%, \tag{8}$$

$$\mathrm{NME} = \frac{1}{N}\sum_{i=1}^{N}\frac{|c_i^e - c_i^o|}{c_i^o} \times 100\%, \tag{9}$$

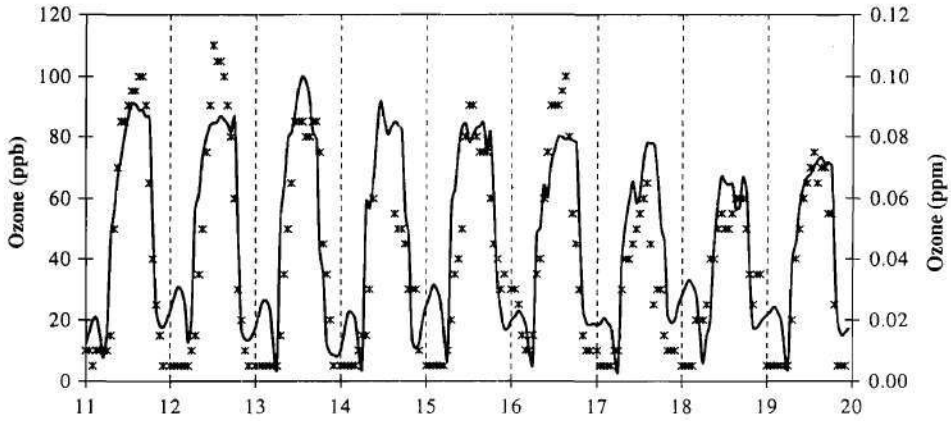

Fig. 2. Observed (•) and simulated (-) ozone levels in Nashville, TN for 11–19 July 1995.

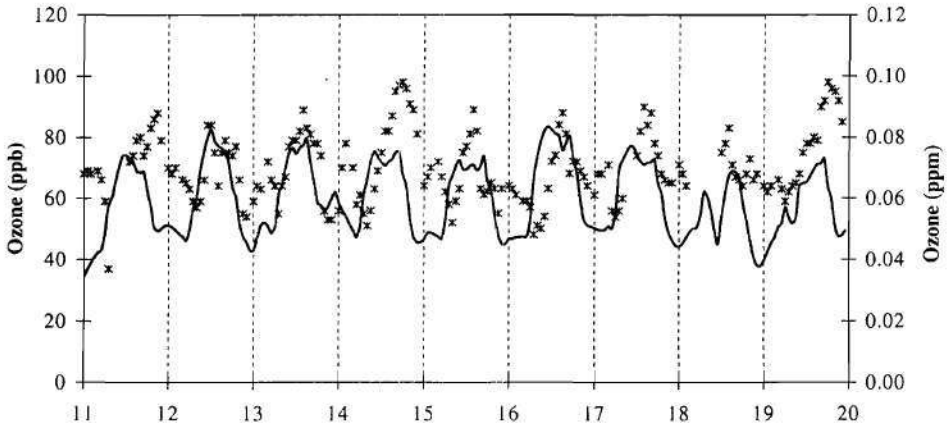

Fig. 3. Observed (•) and simulated (-) ozone levels at GRSM for 11–19 July 1995.

where c_i^e is the model-estimated concentration at station i, c_i^o is the observed concentration at station i, and N equals the number of estimate-observation pairs drawn from all valid monitoring station data for the comparison time period of interest. Since the normalized quantities can become large when the observations are small, a cut-off value of 40 ppb is used in conjunction with Eqs. (8) and (9). Whenever the observation is smaller than the cut-off value, that estimate-observation pair is excluded from the calculations. Table 3 shows a summary of the statistics for each day during the 11–19 July 1995 episode. Note that the normalized biases are within $\pm 15\%$ with the exception of 19 July 1995. The normalized errors are $<25\%$. Both the normalized bias and the normlaized error are within the bounds set by EPA for urban-scale modeling (USEPA, 1991).

5.2. Aerosol performance

Aerosol performance was evaluated by comparing modeling results to observations taken from the IMPROVE monitoring network. IMPROVE measurements are taken on Wednesday and Saturday each week and are reported as a 24-hour average concentration. Therefore, measurements are only available for 3 days during the 11–19 July 1995 episode (12, 15, and 19 July). The species that were compared include fine ($<2.5\,\mu m$) sulfate, fine nitrate, fine ammonium, fine elemental carbon, fine organic carbon, fine soils (crustals), total $PM_{2.5}$, and total PM_{10}. There are 18 IMPROVE monitoring sites in the modeling domain. However, five of those sites are located near or on the boundary of the modeling domain and are easily influenced by the boundary conditions. Therefore, only observations from the remaining 13 stations are used to determine the aerosol model performance. Table 4 lists the resolution of the URM-1ATM grid cells containing these stations.

The four nearest nodes to each IMPROVE station are distance weighted (using bilinear interpolation) to determine the speciated aerosol concentration at each monitoring site. Fig. 4 shows a stacked bar chart comparing the modeled and measured aerosol concentrations for sulfate (SO_4), organics (ORG), ammonium (NH_4), nitrate (NO_3), elemental carbon (EC), soils, and other unidentified aerosol mass. The unidentified mass is mostly related to water associated with the aerosols and/or the assumption that the total organic mass is 1.4 times the organic carbon mass (Andrews et al., 2000). The model results do not contain any unidentified mass. The most abundant species in the fine PM (not including the unidentified mass) is sulfate, followed by organics and ammonium. The largest difference between modeled and observed $PM_{2.5}$ occurs at the Brigantine, NJ site. However, this monitoring station is located in a 48-km grid cell.

Table 5 contains a summary of the normalized mean bias and error for all the stations in the 12, 24, and 48 km grid cells for the 3 days that IMPROVE

Table 3
Ozone performance statistics for the 11–19 July 1995 episode

Date	Norm. mean bias (%)	Norm. mean error (%)
11/7/1995	−3.00	18.82
12/7/1995	4.48	21.08
13/7/1995	−3.46	17.09
14/7/1995	−4.76	20.60
15/7/1995	−2.16	22.16
16/7/1995	13.22	24.37
17/7/1995	12.99	22.99
18/7/1995	−6.17	18.20
19/7/1995	−15.73	22.43

Table 4
IMPROVE and NADP monitoring stations used for performance evaluation

IMPROVE stations and grid resolution	NADP stations (12 km grid resolution)
Brigantine (BRIG), NJ—48 km	Lilley Cornett Woods (KY22), KY
Dolly Sods/Otter Creek (DOSO), WV—12 km	Coweeta (NC25), NC
Great Smoky Mountains (GRSM), TN—12 km	Mt. Mitchell (NC45), NC
Jefferson/James River Face (JEFF), VA—12 km	Walker Branch Watershed (TN00), TN
Lye Brook (LYBR), VT—96 km	Charlottesville (VA00), VA
Mammoth Cave (MACA), KY—24 km	Horton's Station (VA13), VA
Okefenokee (OKEF), GA—96 km	Shenandoah National Park (VA28), VA
Cape Romain (ROMA), SC—48 km	Babcock State Park (WV04), WV
Shenandoah (SHEN), VA—12 km	Parsons (WV18), WV
Shining Rock (SHRO), NC—12 km	
Sipsey (SIPS), AL—12 km	
Upper Buffalo (UPBU), AR—96 km	
Washington (WASH), DC—24 km	

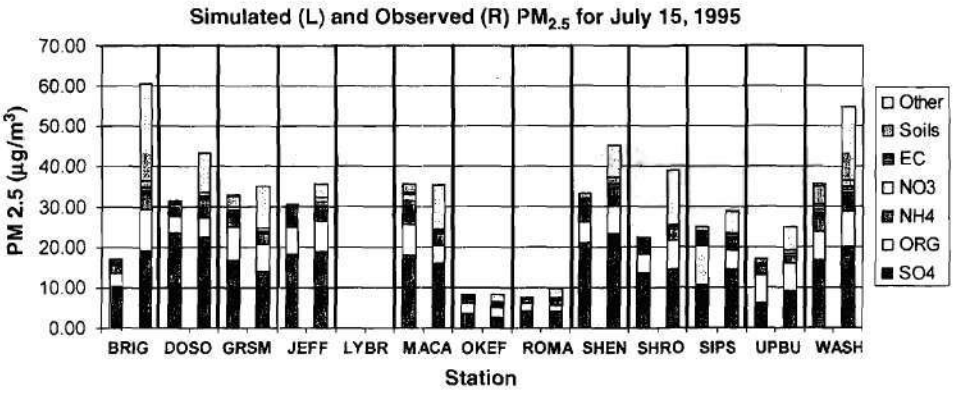

Fig. 4. Simulated (left) and observed (right) speciated $PM_{2.5}$ on 15 July 1995.

Table 5
Mean observations and performance statistics for speciated PM and wet deposition species

Species	Mean observation	NMB (%)	NME (%)
Fine sulfate PM	$10.31\,\mu g\,m^{-3}$	−6.88	18.72
Fine nitrate PM	$0.26\,\mu g\,m^{-3}$	86.59	143.50
Fine ammonium[a] PM	$3.94\,\mu g\,m^{-3}$	−33.41	34.74
Fine organic PM	$4.92\,\mu g\,m^{-3}$	5.60	41.90
Fine elem. carbon PM	$0.71\,\mu g\,m^{-3}$	−17.99	46.39
$PM_{2.5}$	$25.13\,\mu g\,m^{-3}$	−18.85	23.62
PM_{10}	$32.37\,\mu g\,m^{-3}$	−7.24	21.89
Sulfate wet deposition	$64.89\,mg\,m^{-2}$	−14.91	22.02
Nitrate wet deposition	$34.47\,mg\,m^{-2}$	−47.98	48.71
Ammonium wet deposition	$8.02\,mg\,m^{-2}$	34.49	38.20
Hydrogen ion wet deposition	$1.36\,mg\,m^{-2}$	−58.56	61.45
Calcium wet deposition	$2.44\,mg\,m^{-2}$	−42.23	44.02
Magnesium wet deposition	$0.30\,mg\,m^{-2}$	−50.47	50.66
Precipitation	16.48 mm	−60.66	61.26

[a]Ammonium PM from IMPROVE is assumed to be in the form of ammonium sulfate and ammonium nitrate.

measurements were available throughout the episode. A slightly different definition of NMB and NME were used to calculate the performance for aerosols and wet deposition. Eqs. (10) and (11) were used to avoid the problem of unreasonably high biases and error that occur when some of the observations are close to zero:

$$\mathrm{NMB} = \frac{\sum_{i=1}^{N}(c_i^e - c_i^o)}{\sum_{i=1}^{N} c_i^o} \times 100\%, \tag{10}$$

$$\mathrm{NME} = \frac{\sum_{i=1}^{N}|c_i^e - c_i^o|}{\sum_{i=1}^{N} c_i^o} \times 100\%, \tag{11}$$

where c_i^e is the model-estimated concentration at station i, c_i^o is the observed concentration at station i, and N equals the number of estimate-observation pairs drawn from all valid monitoring station data for the comparison time period of interest.

In order to determine $PM_{2.5}$, all the aerosol species for the first three size bins were summed. To determine the PM_{10} concentrations, the coarse aerosol fractions (2.5–10.0 μm) were added to the $PM_{2.5}$ concentrations. There is good agreement between model predictions and observation (<24% normalized mean error) when compared to the gravimetric measurements.

Sulfate (constituting approximately 40% of the fine PM) is biased low by 6.9% and the normalized mean error is 18.7%. The nitrate concentrations are usually quite small ($<1.0\,\mu g\,m^{-3}$); therefore, the normalized error and bias can be very high even though the absolute error is quite low. Ammonium usually is found in the form of ammonium sulfate ($(NH_4)_2SO_4$), ammonium bisulfate (NH_4HSO_4), and ammonium nitrate (NH_4NO_3). The ammonium concentration primarily depends on the amount of sulfate and gas-phase ammonia that is available. There are no direct measurements of ammonium at the IMPROVE stations.

Therefore, for the purpose of ammonium performance evaluation, it has been assumed that the sulfate and nitrate are completely neutralized with NH_4^+. The ammonium aerosol predictions are biased low at most stations and the normalized mean error is <35%. The under prediction in ammonium might be attributed to the assumption that the observed ammonium is fully neutralized as ammonium sulfate. If instead, the measured sulfate was assumed to be ammonium bisulfate, then the model generally overestimated ammonium. Recent ammonium measurements in the Great Smoky Mountains suggest the ammonium is actually a combination of ammonium sulfate and ammonium bisulfate (EPRI, 1998). Incorporation of this information in the performance evaluation would result in a smaller bias and error.

Organics comprise about 20% of the $PM_{2.5}$ mass. The normalized mean bias is 5.6% and the normalized mean error is <42%. Like nitrate, the observations for elemental carbon (EC) are low ($<1.0\,\mu g\,m^{-3}$). However, the performance for EC is better than nitrate because EC is inert and nitrate is very sensitive to small errors in other constituents (e.g., sulfate and ammonium). This is probably because EC is an inert primary emission species. The aerosol species that are lumped into modeled "soils" consist of calcium and "other" PM. Since the modeled species do not correspond to the species defined by IMPROVE, performance statistics were not calculated.

5.3. Wet deposition performance

Wet acid deposition performance was evaluated by comparing modeling results to observations taken from the NADP monitoring network. The species that were compared include sulfate, nitrate, ammonium, hydrogen ion, and crustal cations (Mg and Ca). NADP measurements are taken once each week (Tuesday) and the concentrations and precipitation are reported as a 7-day cumulative. Multiplying the measured concentration by the precipitation results in depositions with units of mass flux. There are 83 NADP monitoring sites in the modeling domain. However, since wet deposition is very localized, only data from the stations in the 12 km grids are used to determine model performance. These stations are listed in Table 4.

Since there is a large spatial variation in precipitation and the RAMS model results do not match observed precipitation at exact locations, the NADP observations are compared to the *best* (i.e., closest to the observation) model result within a 30 km radius from the monitoring site. Fig. 5 shows a comparison of NADP observations for sulfate to the *cell* and *best* model predictions for the 7-day cumulative period of 11–18 July 1995. Although the *cell* values have a tendency to miss the observed sulfate mass flux, the *best* values match well. Station VA00 demonstrates that missing the location of the precipitation by a couple of grid cells leads to large changes in precipitation rates and wet deposition mass fluxes. The average mass fluxes, normalized mean errors, and normalized mean errors for the species undergoing wet deposition are shown in Table 5. Note that the NMB and NME are calculated using the *best* model prediction.

The biases in the wet deposition mass fluxes are highly dependent on the precipitation rates. The simulated mass fluxes for all the species (except ammonium) are biased low, as are the precipitation rates. The ammonium mass fluxes are somewhat higher than the observations due to the under predictions in the hydrogen ion mass fluxes.

6. Conclusions

URM-1ATM was evaluated for the 11–19 July 1995 episode using RAMS and EMS-95 for meteorological and emission inputs, respectively. The normalized mean biases and errors for ozone were generally $< \pm 15\%$ and

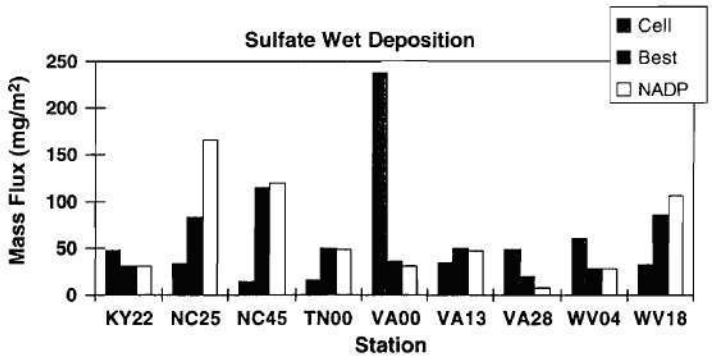

Fig. 5. Simulated and observed wet deposition of sulfate for the week of 11–18 July 1995.

25%, respectively. The model generally under predicted the daytime peaks but the diurnal variations and the timing of the peaks did conform well with observations. The IMPROVE measurements for aerosols contained an unidentified mass component that makes comparisons to organic PM and gravimetric PM measurements difficult. However, the major aerosol constituents of fine PM (sulfate, ammonium, and organic carbon) generally had normalized mean errors <40%. It was found to be extremely difficult to model the spatial distribution and magnitude of the precipitation. The wet deposition fluxes of most species were biased low due to an under prediction in precipitation. However, the normalized mean errors for sulfate, nitrate, and ammonium wet deposition fluxes are still <50%. Finally, a new observation-based interpolation scheme was developed for setting initial and boundary conditions. It was observed that all the modeling results were sensitive to the boundary conditions and that long-range transport of both gas and aerosol species from the boundary can affect the concentrations of pollutants thousands of kilometers away.

Acknowledgements

This research was sponsored by the Southern Appalachian Mountain Initiative (SAMI) and the Environmental Protection Agency in grants to Georgia Institute of Technology and California Institute of Technology. The authors gratefully acknowledge Dr. Spyros Pandis (Carnegie Mellon University) for supplying the aerosol module, Dr. Carl Berkowitz (Pacific Northwest Laboratory) for supplying the wet scavenging module, and Dr. Rick Saylor (Georgia Institute of Technology) for helping to integrate the scavenging module into URM.

References

Andrews, E., Saxena, P., Musarra, S., Hildemann, L.M., Koutrakis, P., McMurry, P.H., Olmez, I., White, W.H., 2000. Concentration and composition of atmospheric aerosols from the 1995 SEAVS experiment and a review of the closure between chemical and gravimetric measurements. Journal of Air and Waste Management Association 50, 648–664.

Ansari, A.S., Pandis, S.N., 1999. Prediction of multicomponent inorganic atmospheric aerosol behavior. Atmospheric Environment 33, 745–757.

Berkowitz, C.E., Easter, R.C., Scott, B.C., 1989. Theory and results from a quasi-steady-state precipitation-scavenging model. Atmospheric Environment 23, 1555–1571.

Byun, D.W., Ching, J.K.S., 1999. Science Algorithms of the EPA Models-3 Community Multiscale Air Quality (CMAQ) Modeling System. EPA/600/R-99/030. US Environmental Protection Agency, Office of Research and Development, Washington, DC.

Carter, W.P.L., 1990. A detailed mechanism for the gas-phase atmospheric reaction of organic compounds. Atmospheric Environment 24, 481–518.

Carter, W.P.L., 1995. Computer modeling of environmental chamber measurements of maximum incremental reactivities of volatile organic compounds. Atmospheric Environment 29, 2513–2527.

Doty, K.G., Tesche, T.W., Timin, B., 2001. Meteorological modeling for the Southern Appalachian initiative. Final Report, Southern Appalachian Mountain Initiative, Asheville, NC.

EPRI, 1998. Southeastern aerosol and visibility study (SEAVS): concentration and composition of atmospheric aerosols at Look Rock, Tennessee, July–August 1995. Report TR-111063, Electric Power Research Institute, Palo Alto, CA.

Gelbard, F., 1990. Modeling multicomponent aerosol particle growth by vapor condensation. Aerosol Science Technology 12, 399–412.

Green, P.J., Sibson, R., 1978. Computing dirichlet tessellations in the plane. The Computer Journal 21, 168–173.

Harley, R.A., Russell, A.G., McRae, G.J., McNair, L.A., Winer, D.A., Odman, M.T., Dabdub, D., Cass, G.R., Seinfelf, J.H., 1992. Continued development of a photochemical model and application to the Southern California air quality study (SCAQS) intensive monitoring period: phase I. Final Report to Coordinating Research Council.

Kalnay, E., Kanamitsu, M., Kistler, R., Collins, W., Deaven, D., Gandin, L., Iredell, M., Saha, S., White, G., Woollen, J., Zhu, Y., Chelliah, M., Ebisuzaki, W., Higgins, W., Janowlak, J., Mo, K.C., Ropelewski, C., Wang, J., Leetmaa, A., Reynolds, R., Jenne, R., Joseph, D., 1996. The NCEP/NCAR 40-year reanalysis project. Bulletin of the American Meteorological Society 77, 437–471.

Kim, Y.P., Seinfeld, J.H., 1990. Simulation of multicomponent aerosol condensation by the moving sectional method. Journal of Colloid and Interface Science 135, 185–199.

Kumar, N., Russell, A.G., 1996. Multiscale air quality modeling of the Northeastern United States. Atmospheric Environment 30, 1099–1116.

Kumar, N., Odman, M.T., Russell, A.G., 1994. Multiscale air quality modeling: application to Southern California. Journal of Geophysical Research 99, 5385–5397.

Mueller, P.K., 1998. NARSTO 1998 model-intercomparison study verification data: NARSTO-northeast 1995 surface ozone, NO, and NO_x. Available online from the Langley Atmospheric Sciences Data Center (http://eosweb.larc.nasa.gov/), NASA Langley Research Center, Hampton, VA, USA.

National Center for Atmospheric Research, 1982. Regional Acid Deposition: Models and Physical Processes, Boulder, CO.

NPS, 2000. National Park Service Air Quality Research Division Fort Collins. Anonymous ftp at ftp://alta_vista.cira.colostate.edu in/data/improve.

Nenes, A., Pilinis, C., Pandis, S.N., 1998. Isorropia: a new thermodynamic equilibrium model for multiphase multicomponent inorganic aerosols. Aquatic Geochemicals 4, 123–152.

Odman, M.T., Russell, A.G., 1991a. Multiscale modeling of pollutant transport and chemistry. Journal of Geophysical Research 96, 7363–7370.

Odman, M.T., Russell, A.G., 1991b. A multiscale finite element pollutant transport scheme for urban and regional modeling. Atmospheric Environment 25A, 2385–2394.

Odman, M.T., Russell, A.G., 1993. A nonlinear filtering algorithm for multi-dimensional finite element pollutant advection schemes. Atmospheric Environment 27A, 793–799.

Odman, M.T., Russell, A.G., 2000. Mass conservative coupling of non-hydrostatic meteorological models with air quality models. In: Gryning, S.-E., Batchvarova, E. (Eds.), Air Pollution Modeling and its Application XIII. Kluwer Academic/Plenum Publishers, New York, NY, pp. 651–660.

Pechan/Avanti Group, 2001. Southern Appalachian Mountains initiative (SAMI) emissions projections to 2010 and 2040: growth and control data and emission estimation methodologies. Draft Final Report No. 01.07.002/9405.000.

Pandis, S.N., Harley, R.A., Cass, G.R., Seinfeld, J.H., 1992. Secondary organic aerosol formation and transport. Atmospheric Environment 26A, 2269–2282.

Pandis, S.N., Wexler, S.W., Seinfeld, J.H., 1993. Secondary organic aerosol formation and transport—II. Predicting the ambient secondary organic aerosol size distribution. Atmospheric Environment 27A, 2403–2416.

Pielke, R.A., Cotton, W.R., Walko, R.L., Tremback, C.J., Lyons, W.A., Grasso, L.D., Nicholls, M.E., Moran, M.D., Wesley, D.A., Lee, T.J., Copeland, J.H., 1992. A comprehensive meteorological modeling system—RAMS. Meteorological Atmospheric Physics 49, 69–91.

Pierce, T.E., 1996. Documentation for BEIS2 located at ftp://monsoon.rtpnc.epa.gov/pub/beis2/SOS/AAREADME.

Pierce, T.E., Geron, C.D., 1996. The personal computer version of the biogenic emissions inventory system (PCBEIS2.2). AAREADME, anonymous ftp at monsoon.rtpnc.epa.gov located in/pub/beis2/pcbeis22.

Pierce, T.E., Lamb, B.K., Van Meter, A.R., 1990. Development of a biogenic emissions inventory system for regional scale air pollution models. In: Proceedings of the 83rd Annual Meeting of the Air and Waste Management Association, Pittsburgh, PA.

Preparata, F.P., Shamos, M.I., 1985. Computational Geometry: An Introduction. Springer, Berlin.

Russell, A.G., Dennis, R., 2000. Narsto critical review of photochemical models and modeling. Atmospheric Environment 34, 2283–2324.

Russell, A.G., Winter, D.A., McCue, K.F., Cass, G.R., 1990. Mathematical modeling and control of dry deposition flux of nitrogen-containing air pollutants. Report on CARB A6-188-32. California Air Resources Board, CA.

Scott, B.C., 1987. User's Manual for the Convective Cloud Module Version 1.0. PNL-6188. Pacific Northwest Laboratory. Richland, WA.

Seinfeld, J., Pandis, S., 1998. Atmospheric Chemistry and Physics. Wiley, Inc., New York, NY.

USEPA, 1991. Guidance for Regulatory Application of the Urban Airshed Model (UAM), Office of Air Quality Planning and Standards, US Environmental Protection Agency, Research Triangle Park, NC.

USEPA, 1994. User's Guide to MOBILE5 (Mobile Source Emission Factor Model). EPA-AA-TEB-94-01. US Environmental Protection Agency, Office of Air and Radiation, Office of Mobile Sources, Emissions Planning and Strategies Division, Air Quality Analysis Branch, Ann Arbor, MI.

USEPA, 2001. EPA AIRS Data. US Environmental Protection Agency, Office of Air Quality Planning & Standards, Information Transfer & Program Integration Division, Information Transfer Group. www.epa.gov/airsdata.

Wesely, M.L., 1989. Parameterization of surface resistances to gaseous dry deposition in regional-scale numerical models. Atmospheric Environment 23, 1293–1304.

Wilkinson, J.G., Loomis, C.F., McNally, D.E., Emigh, R.A., Tesche, T.W., 1994. Technical Formulation Document: SARMAP/LMOS Emissions Modeling System (EMS-95). AG-90/TS26 & AG-90/TS27. Alpine Geophysics, Pittsburgh, PA.

Zhang, Y., Seigneur, C., Seinfeld, J.H., Jacobson, M.Z., Binkowski, F.S., 1999. Simulation of aerosol dynamics: a comparative review of algorithms used in air quality models. Aerosol Science Technology 31, 487–514.